Mapping of Total Suspended Sediments Using Meteosat Second Generation

1 author:

Jane Ndungu
Kenya Marine and Fisheries Research Institute (KMFRI)
9 PUBLICATIONS **26** CITATIONS

SEE PROFILE

Mapping of Total Suspended Sediments Using Meteosat Second Generation

Jane Ndungu
February, 2009

Mapping of Total Suspended Sediments Using Meteosat Second Generation

by

Jane Ndungu

Thesis submitted to the International Institute for Geo-information Science and Earth Observation in partial fulfilment of the requirements for the degree of Master of Science in Geo-information Science and Earth Observation, Specialisation: (fill in the name of the specialisation)

Thesis Assessment Board

Chairman: Prof. Dr. Ing. W. Verhoef

External Examiner: Dr. van der Woerd (Vrije Universiteit Amsterdam)

Supervisor(s):

Dr. Ir. Mhd. S. Salama (Departement of Water Resources, ITC)

Dr. B.H.P. Maathuis (Departement of Water Resources, ITC)

INTERNATIONAL INSTITUTE FOR GEO-INFORMATION SCIENCE AND EARTH OBSERVATION
ENSCHEDE, THE NETHERLANDS

Disclaimer

This document describes work undertaken as part of a programme of study at the International Institute for Geo-information Science and Earth Observation. All views and opinions expressed therein remain the sole responsibility of the author, and do not necessarily represent those of the institute.

Abstract

High sediment load significantly reduces the optical transparency of coastal waters and causes establishment of sediments shoals that affects navigation. In addition, Total Suspended Sediments (TSS) affect adversely primary productivity and ecology by transporting chemicals and re-suspended pollutants. Therefore, estimation of the sediment concentration levels and dynamics of sediment distribution along coastal environment is essential for improvement of integrated resource management especially in maintaining safe navigation routes, harbour access and dredging operations. Whereas most studies have been successful in retrieval of the suspended particulate matter, the rapid fluctuations in TSS concentrations at coastal environment calls for higher temporal resolution which has not been widely addressed. The current study envisaged to achieve this using SEVIRI Instruments on board Meteosat Second Generation (MSG) satellite using channel one and two (visible bands).

With the objective of retrieving TSS, an algorithm comprised of three models (Gordon, 1975; 1988 and Morel and Prieur (1977) was formulated in Matlab 7.6.0 software to compute water leaving radiance; normalized water leaving radiance; the exact water leaving radiance; subsurface irradiance reflectance; and bio-optical modeling (parameterization of inherent optical properties) and finally TSS concentration, respectively. Data preparation involved cloud and sun glint masking. The coded algorithm determined TSS concentration from Global MSG images, which were validated along the Kenyan Coast (Sabaki River Estuary).

The results from Gordon (1975) model resulted in negative values because backscattering was larger than absorption. A scatter plot of the TSS concentration (lab) versus Gordon et al., (1988) model for small particles showed two clustered plots corresponding to neaptide and springtide; a regression analysis of 85%, correlation coefficient of 0.92 and absolute Root Mean Square Error (RMSE) of 3.44 mg/m^3. Though the large particles indicated the same correlation coefficient of 0.92, RMSE was $2.73mg/m^3$. Regression analysis of Morel and Prieur, (1977) model was 85%, correlation coefficient of 0.92 for both large and small particles. However, the absolute RMSE showed significant differences between small (2.81 mg/m^3)and the large (12.08 mg/m^3) particles.

A spatial-temporal assessment of the TSS along the Kenyan Coast indicated three distinct trends in TSS concentration: marked low concentration for sites close to the land; an increasing sediment concentration seawards and an anomalously high concentration along the river mouth with a gradual decrease in seaward direction. A statistical test showed that there was no significant difference between the modelled and insitu TSS concentrations. These results attest to the novelty of the models used in the algorithm for monitoring TSS concentration along the coastal environment at near-real time-resolution of 15 minutes. Consequently, it was concluded that it is possible to monitor TSS concentration using SEVIRI instruments on board Meteosat Second Generation.

I dedicate this piece of work to

My Family

Acknowledgements

The success of this research was attributed to various contributions. First and fore most, I would like to acknowledge NUFFIC for the awarding me a scholarship to study in Netherlands, including all the financial support. Am obliged to thank the International Institute for Geoinformation and Earth Observation for providing the knowledge and skills needed to carry out this study to a completion in a conducive environment for learning and opening a door to a society of cultural and social diversity.

Special gratitude goes to my supervisors Dr. ir Suhyb Salama, and Dr. Ben Mathias for their tireless efforts, valuable comments and accommodative nature in ensuring the success of this research. I would also like to thank my course Director Dr. Micheal Weir for his support as well as the smooth overall coordination. I also owe Joris Timmermans special appreciation to the support he offered. Without you all this would not have been a success.

Special appreciation goes to my colleagues in ITC who have been of great support both socially and morally, particularly my Kenyan friends.

Am indebted to acknowledge Kenya Marine and Fisheries Research Institute for the fieldwork support provided.

Special thanks go to my family for their prayer, support and encouragement within the last 18 months. To you all I say God bless you.

I thank Almighty God for seeing me through these studies in stable health and sound mind.

Table of contents

List of figures

List of tables

1. Introduction

1.1. Back Ground Information

Over the years, researches on Total suspended sediments (TSS) retrieval from the remote sensed data have been carried out. These studies range from use of one band (665 nm) to extract mineral suspended sediment concentrations (Binding *et al*, 2005); two bands (580-680 and 720-1100 nm) for Advanced Very High Resolution Radiometer (AVHRR) by Yan, *et al*., 1998); three wavelengths (R 412, 490 and 555 by (Hoge and Lyon, 2005); four bands for sea-viewing Wide Field of view Sensor (Warrick, *et. al*., 2004); to more advanced hyperspectral studies such as CASI hyperspectral airborne remote sensing (Sterckx and Debruyn, 2004). Pierson and Strombeck (2001) used in situ hyperspectral reflectance just below the water surface, a set of measured inherent optical properties, and concentrations of optically active substances to construct a bio-optical model of Lake Mälaren, Sweden. Multispectral and broad band resolutions have as well been demonstrated (Chernetskiy, *et al.,* 2009; Antoine and Morel 1999; Dekker *et al.,* 1998). Whereas most of these studies have been very successful, the rapid fluctuations in Total Suspended Sediments concentrations at coastal environment call for higher temporal resolution which has not been widely addressed.

The current study envisaged to bridge the high temporal resolution gap using SEVIRI Instruments (Spinning Enhanced Visible and InfraRed Imager) on board Meteosat Second Generation (MSG) satellite. This is a geostationary satellite widely used as a weather satellite. It has a capability of observing the earths' full disk at 15 minutes repeat cycles with 12 spectral channels (*Table* 1) at 3 km, 5 km and 1km spatial resolution at nadir in the visible, Infrared and high resolution visible respectively (ESA, 2004). The strategic position of the MSG visible bands in the near infrared makes it sufficient in as far as retrieval of total suspended sediments is concerned. Besides, Suspended Particulate Matter extraction from two bands of AVHRR (Advanced Very Hugh Resolution Visible) particularly in the near infrared region has been proved to be effective (Stumpf and Pennock, 1989; Yan *et al*., 1997). This is through retrieval of the water-leaving reflectance by assuming spatial homogeneity in the infrared region (Ruddick *et al.,* 2000; Gordon and Boynton, 1997). Including a band in the near infrared enhances the retrieval of the water leaving reflectance (Ruddick *et al.,* 2000). In this study, Gordon *et al.,* (1988); Gordon *et al.,* (1975); and Morel and Prieur, (1977) bio-optical models were evaluated for their effectiveness in retrieving the Total suspended Sediments from Meteosat Second Generation.

Application of SEVIRI instrument, on board Meteosat second generation satellites in estimating sediment distribution has not been broadly done. Successful retrieval of the Total Suspended Sediments distribution from MSG would lead to enhanced understanding of its dynamics at near-real time basis or precisely at 15 minutes temporal resolutions. Thus, enhance integrated resource management.

1.2. Problem Statement/ rationale

Fine-grained cohesive and non-cohesive sediments characterize a wide range of coastal environments (Healy *et al*., 2002; Winterwerp and Van Kesteren, 2004). These sediments load results from continental erosion as well as hydrologic processes that vary with respect to various factors such as climatic (precipitation, rainfall intensity) as well as morphological parameters (Wolfgang and Probst, 1996). These conditions are highly variable both in time and space. At estuarine region, in particular, discharge of the river into the ocean results in reduction in salinity as fresh river water mixes with ambient saline water. It also results in ingression of particulate and suspended matter, such as sediments, pollutants, organics and nutrients. Of particular importance is the high sediment discharge that significantly reduces the optical transparency of coastal waters and causes establishment of sediments shoals that affects navigation (De Kok, 1992; Mishra, 2004). In addition suspended particulate matter (SPM) affects adversely primary productivity and ecology by transporting chemicals and resuspended pollutants. Moreover, its organic component forms a major component of carbon cycle (Laane *et.al.*, 1999); Turner and Millward, 2002).

Estimation of the spatial-temporal sediment distribution along coastal environment is essential in improvement of integrated resource management especially in maintaining safe navigation routes, harbour access and dredging operations (De Kok, 1992). Seasonal variations of Total suspended Sediments are clearly visible in the satellite images. However, the short term variations (tidal, spring-neap tidal cycle) have not been widely achieved. This study attempts to achieve high temporal estimation of total suspended sediments by applying the SEVIRI instrument, on board Meteosat second generation satellites. This is because it has a very high temporal resolution of 15 minutes with two visible bands (ESA, 2004).

In Sabaki River in particular (validation site) suspended sediments have affected the marine ecosystem along the Kenya Coast to a great extent. This is because the changing land-use practices in

the rivers' catchment basins, has increased river-sediment discharge into coastal waters (McClanahan and Obura 1997) thereby causing extensive physical alteration and destruction of the ecosystem (UNEP/GPA 2004).

1.3. Objectives

1.3.1. Main Objective

The objective of this research is to obtain a model for MSG to estimate the concentration of total suspended sediments.

1.3.2. Specific Objectives

- Obtain a model to atmospherically correct (AC) MSG -SEVIRI image for aerosol reflectance and water vapour transmittance.
- Carryout atmospheric correction on MSG images.
- Obtain a model and retrieve the concentration of suspended sediment from MSG-SEVIRI
- Validate the results with in-situ measurements.

1.4. Research questions

- Is the suggested Atmospheric Correction method able to retrieve water leaving radiance from MSG-SEVIRI?
- Is the obtained bio-optical technique effective in mapping suspended sediments using MSG-SEVIRI visible bands?
- Does the high temporal resolution of MSG-SEVIRI derived products improve our understanding about the temporal variability of suspended sediment in SEVIRI's field of view?

1.5. Hypothesis

- SEVIRI –MSG visible cannot be used to estimate suspended sediments distribution.

1.6. Research Approach

To achieve the goals a summary of the approach taken is shown on the flowchart below.

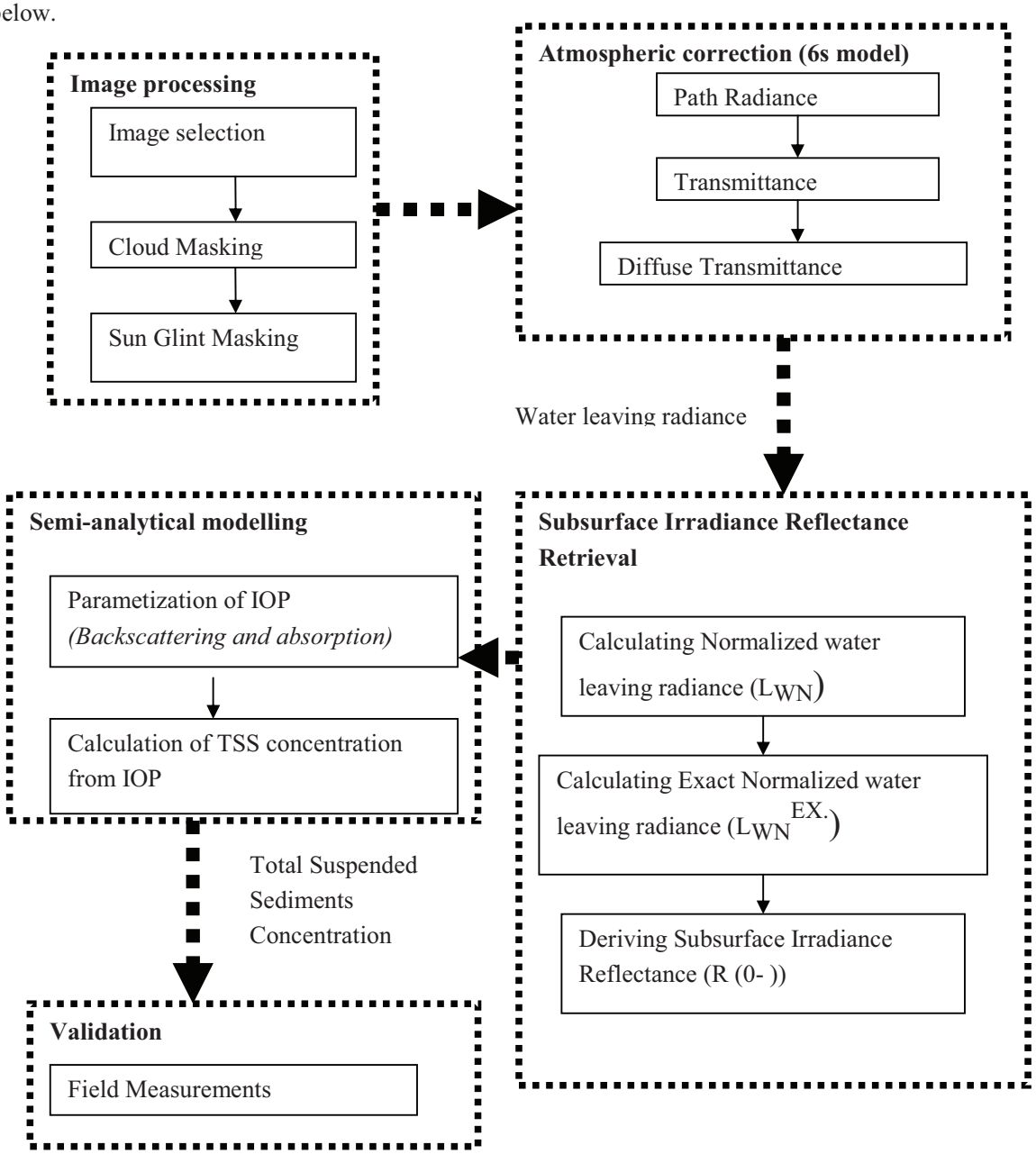

Figure 1 Flow chart of the research approach.

2. Literature Review

2.1. Hydro-optics principles

Hydrologic optics according to Preisendorfer (1976) is a part of the broader discipline known as geophysical optics and is defined as "quantitative study of the interaction of radiant energy with hydrosols especially the natural hydrosols of the earth such as sea, lakes, ponds, rivers, and bays". Preisendorfer (1976), together with Jerlov, (1976) and Austin (1974), formulated the firm physical basis defining the inherent and apparent optical properties of marine water. Mobley (1994) categorized the optical study of marine water into radiative transfer theory and optical oceanography. The radiative transfer theory, which is build from aspects of radiant flux, scattering, absorption, volume area, and length deals with the mathematical treatments of radiative transfer theory (hydro optics) and descriptive optical oceanography (Marine optics).

Mueller and Austin (1992, 1995) formulated Ocean Optics Protocols. Due to the extensive and diverse studies among many authors, the National Aeronautics and Space Administration (NASA), during the period 1985 to 1991, initiated a series of successive science working groups that developed Ocean Optics Protocols for Satellite Ocean Color Sensor Validation document as described by Mueller and Fargion (2002); Fargion and Mueller (2000); Mueller and Austin (1992, 1995) in order to stream line concepts, methods and conventions.

The basic principles underlying hydro optics of the sea water are based on its inherent and apparent properties. The inherent optical properties refers to quantities that define how a light propagating through a point in a medium is modified by its absorption and scattering processes, as first described by Preisendorfer (1960). These properties of the media are independent of geometric properties of the vector light field.

In contrary Apparent Optical properties are based on spectral irradiance and radiance measurements through a medium that are dependent on geometrical distribution of the light field and inherent optical properties of the medium(Mobley, 1994). These properties vary with illumination geometry such variations in solar azimuth and zenith angle. Interactions of surface boundary conditions and IOP define the bidirectional character of remote sensing reflectance of the ocean (Muller et al, 2003c).

2.2. Bio-optical Modelling

Bio-optical modelling methods include: empirical, model based inversion (non-linear optimization and neural network approach), algebraic and semi-analytic radiative transfer models. The empirical algorithms (Clark *et. al*., 1980; Ahn *et. al*., 2001) are simple, easy to derive, implement and test but are always regional in scope and sensitive to changes in water constituents', particularly, seasonal effects. Model based inversions such as non-linear optimization technique (Garver and Siegel, 1997; Maritorena *et. al*., 2002), involves inversion of a forward reflectance model by minimizing differences between calculated values and measured reflectance by changing input variables. Neural network approach (Doerffer *et. al*., 2002) is formulated based on powerful multiple non-linear regression techniques, where the ability of each network to retrieve concentrations depends on model used to produce training sets. Algebraic inversion entails use of algebraic expression that relate semi-analytic models to geophysical products derived, which results into a set of algebraic equations that can be solved to obtain each of unknown components of the model (Loisel and Stramski, 2000). A reputable semi-analytical bio-optical model was used for inverting SeaWiFS data by Garver and Siegel (1997); Maritorena, *et al.,* (2002); and Chomko *et al*., (2002) which account for the three optically significant water constituents; colored dissolved organic matter, chlorophyll and suspended sediments. In this study, Gordon *et al.,* (1988); Gordon *et al.,* (1975); and Morel and Prieur, (1977) bio-optical models were evaluated for their effectiveness in retrieving the Total suspended Sediments from Meteosat Second Generation. This was because they have been widely used and hence the determination of the constants attributed their operation has been done. These constants have as well been tested through research. Ruddick *et al*., (2000) successfully used Gordon *et al*., (1988) model. Mishra (2004) was successful in applying the Morel and Prieur, (1977) while Eleveld *et al*., (2008) has implemented the Gordon *et al.,* (1975) model.

2.2.1. Water leaving Radiance

The remote sensors record a contribution of the water, white caps, sun glint and the atmospheric constituents. The amount of the radiance which is of interest in ocean color remote sensing is about 1-15 % (water leaving Radiance) (Dekker, *et al*., 2001). By definition, water leaving radiance is a radiometric quantity which refers to the radiance that emerges from the water (Muller, *et al.,* 2003[b]). It originates from in-water upward radiance just beneath the interface. Its transfer is governed by reflection and refraction processes which have angular dependencies, namely: Azimuth and Zenith angels for above-water radiances as well as the nadir angle for the in-water (upward) directions. An increase in solar zenith angel leads to a decrease in solar irradiance that is back scattered out of the ocean. Hence surface reflection has to be accounted for in both remote sensed and insitu water leaving

measurements (Wang, 2006). This is done after atmospheric correction and normalization of the water leaving radiance to get the Exact Normalized Water Leaving Radiance. Atmospheric correction involves removal of water, white caps, sun glint and the atmospheric constituents' effects from the remote sensed energy (Gordon, 1997). In this study, the effect of the white caps was assumed to be negligible due to the averaging that due to large spatial resolution (Gordon, 1997) while the sun glint effect was masked. The 6s model for atmospheric correction was found to be efficient in this study since its pixel by pixel based.

Table 1 Table showing the MSG spectral bands and their width

Channel Number	Spectral Band	Band Width (μ um)		
		Centre	**Min.**	**Max.**
1	VIS 0.6	0.635	0.56	0.71
2	VIS 0.8	0.81	0.74	0.88
3	NIR 1.6	1.64	1.50	1.78
4	IR 3.9	3.90	3.48	4.36
5	WV 6.2	6.25	5.35	7.15
6	WV 7.3	7.35	6.85	7.85
7	IR 8.7	8.70	8.30	9.1
8	IR 9.7	9.66	9.38	9.94
9	IR 10.8	10.8	9.80	11.80
10	IR 12.0	12.00	11.00	13.00
11	IR 13.4	13.40	12.40	14.40
12	HRV	**Broad band (0.4-1.1)**		

Source: Modified from Eumetsat website (ESA, 2004)

3. Fieldwork

3.1. Validation Site

To validate the results of the total suspended sediments retrieved from MSG, Sabaki (or Athi-Galana-Sabaki) river estuary was chosen. It's situated along the Kenyan Coast between longitudes 39^0 50' E and 40^0 20' E and latitudes 3^0 0'S and 3^0 20' S. It is the mouth of the second largest river in Kenya which is 650 km long with a catchment of 70,000km^2 extending from the Kenyan highlands to southern Ungwana Bay, north of Malindi (Obura, 2001) (see figure 2). It covers about 11% of the Kenyan area. Rainfall in the catchment ranges between 500 and 1500 mm per annum while evaporation ranges between 1700 and 2000 mm per annum. The rainfall which is bi-modal is influenced by Southern (associated with long rains between March and June with a peak in April at the highlands) and Northern monsoons (associated with the short rains that occur between November and December with the peak in November) (Ojany and Ogendo, 1986), although there are inter-annual variations associated with El-Nino and La-Nina southern oscillation phenomena. This rainfall leads to increased water discharge as well as sediment loads associated with the Sabaki river basin, particularly from the Kenyan highlands into the Indian Ocean. This hinders establishment of coral complexes in the southern region of Ungwana Bay (KMFRI, 2002).

The Kenyan coast experiences a semi diurnal tidal regime which varies from 1.5 to 4m amplitude from neap to spring tide. These creates vast intertidal platform and rocky shore communities that are exposed twice daily during low tides. In general the salinity regime is moderate with high nutrients level from terrestrial runoff and ground water. The Kenyan Marine environment is characterized by warm conditions whose temperatures are in the range of 25-31 degrees centigrade (Obura, 2001). Under these conditions, Sabaki river estuary is not an exception.

Being a major agricultural, industrial and urban area, Sabaki River basin is considered of great economic importance. However, the changing land-use practices in the rivers' catchment basins, has increased river-sediment discharge into coastal waters (McClanahan, 1997) thereby causing extensive physical alteration and destruction of the ecosystem (UNEP/GPA, 2004). Among other activities, Land use intensification, steep slopes cultivation, deforestation, urban sprawl and increasing road network may have contributed to high soil Erosion in the high land. This translates to high suspended sediments at River Sabaki Estuary.

Previously, conventional means of suspended sediments monitoring has been used in the Kenyan coast region (Brakel, 1984; McClanahan and Obura, (1997); Kitheka et al., (2003); Kitheka *et al*., (2005); McClanahan *et al.*, 2005). However, no bio-optical modelling has been used in this region for retrieval of suspended sediments.

3.2. Sabaki Sediment Regime

Seasonal variability in the discharge from Sabaki River is highly dynamic such that it can transport over 80% of the annual sediment loads within a few days (Dune, 1979). However, during the dry season, flow and sediment discharge can approach zero (Obura, 2001). High sediments flux is experienced in May and November which is as a result of short rains which occur in October to December and long rains in March to May in the Kenyan highlands (KMFRI, 2000). On onset of the rains in the highlands, a delay of one month is experienced before the discharge and sediments peaks in River Sabaki Estuary (KMFRI, 2000). Sediments flux was estimated to be in the range of 7.5 to 14.3 million tonnes translating to annual soil Erosion rate of 110-210 tonnes per kilometer squared (katwijk et al., 1993). The southern monsoon winds influence the sediments plume pushing it to southward to the coral site thereby hindering visibility in the Malindi/Watamu national November and February while northern monsoon winds transports the plume away from the Malindi reef (McClanahan and Obura, 1997). The plume transport phenomenon hinders the tourism business which is of great economic value to the inhabitants.

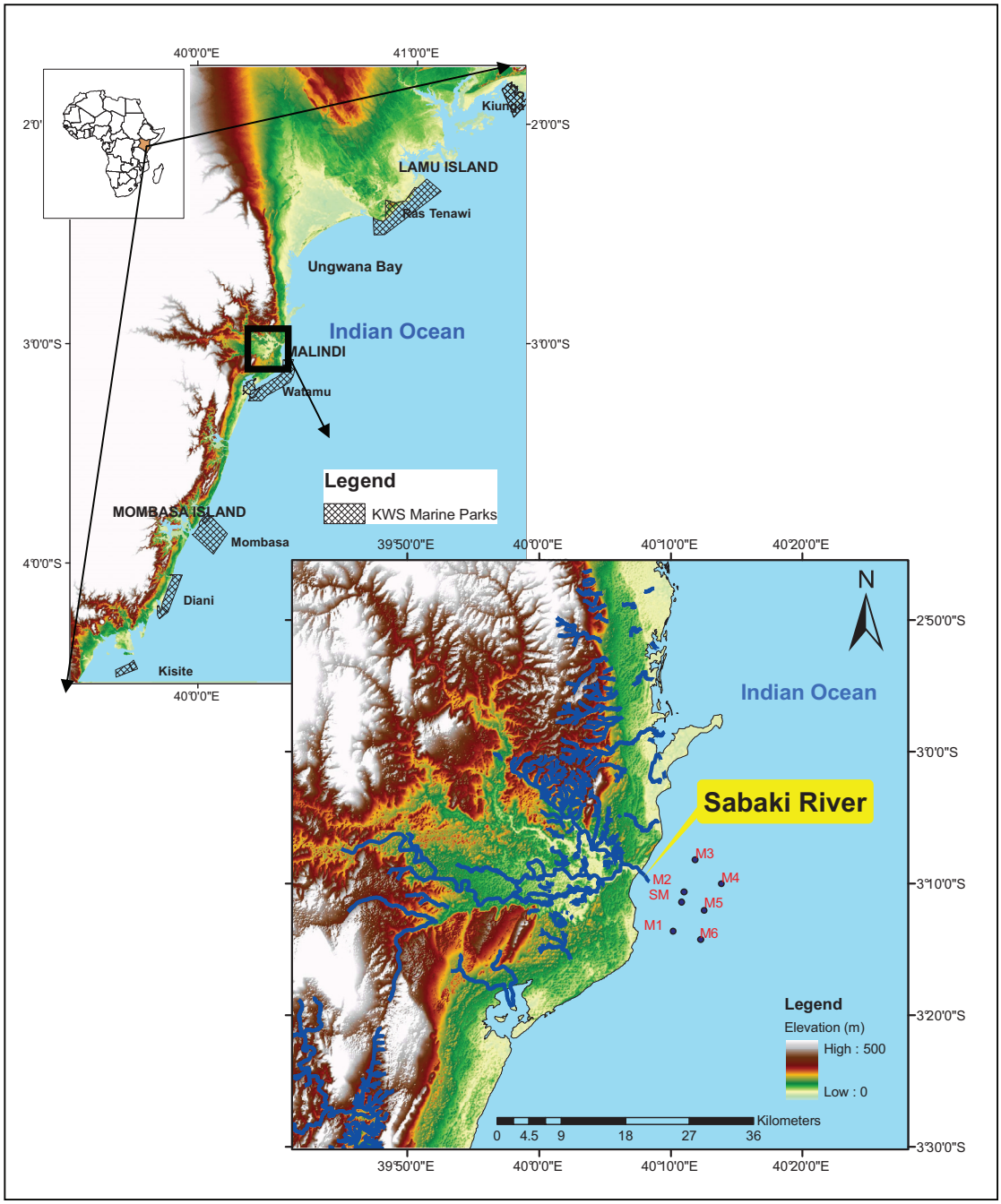

Figure 2 **Map showing the location of Validation site (Sabaki River Estuary along the Kenyan coast)**

3.3. Field Data Collection

The data collected in the field included water samples to determine Total Suspended Sediments, secchi disk depth, bottom depth, salinity, chlorophyll, current speed, GPS points and time. All these parameters were determined at each sampling site i.e corresponding to each independent sample. A detailed description of how each of the data was collected is shown below.

3.3.1. Total Suspended Sediments concentration Measurements

3.3.1.1. Materials and Equipments

- Sampling bottles
- Drying oven
- Glass filter(GFC filters)
- Weighing balance
- Vacuum pump filtration system
- Graduated cylinder
- Aluminum dishes

3.3.1.2. Determination of Total suspended Sediments

To validate the concentration of suspended sediments retrieved from Meteosat Second Generation, field data collection was carried out from 18th of October, 2008 to 25th November, 2008 between 12.00 and 17.00 hours GMT in Sabaki River Estuary in Kenya (Figure 2). Sampling was done from seven stations at an interval of five kilometres transects distance (chosen in accordance to plume movement: North, south and along the river which is influenced by SE and NW monsoons) (KMFRI, 2002). To reduce possibility of chance variations, the sampling was repeated (Moore *et al.*, 2003) for four days during spring tide and three days during neap tide (See appendix 4). A total of 49 independent samples were collected in triplicates. The sites were accessed using a boat. Two litres bottles were used to collect the sea water samples from the selected sites and transported to the

laboratory. Due to high concentrations of TSS, only one litre of water was used for the filtration process. The samples were thoroughly shaken and poured into a graduated cylinder to measure the volume. Filtration onto a prewashed and gravimetrically (Giulietta, *et al.,* 2000) pre-weighed GF/C filters (Short and Coles, 2001; Strickland and Parsons, 1972) (used due to their ability to retain particles as small as 0.4 um in diameter) was done using a vacuum filtration unit. The filters were then removed using forceps and placed in a labelled dish. This was repeated for all the samples. The samples were then placed in a drying oven till they attained a constant weight after which reweighing was done and the new weight recorded. The TSS was then calculated by subtracting the weight of the filter from the final dry weight (filter + TSS).

3.4. Turbidity

Water clarity may be attributed to the amount of the total suspended sediments in the water. In this study, it was determined using a Secchi disk which measures how deep a person can see into the water. In this study it was ensured that all the readings were taken by one person. This was to reduce errors associated with difference in eyesight from one person to another. The readings were done by lowering the Secchi disk into the water while unwinding the waterproof tape attached to it until the observer loses its sight. The disk was then raised until it reappears. The depth of the water where the disk vanishes and reappears is the Secchi disk reading. The depth level reading on the tape at the surface level of the water was recorded to the nearest meter. The figure 3 below shows the illustration how the readings were taken.

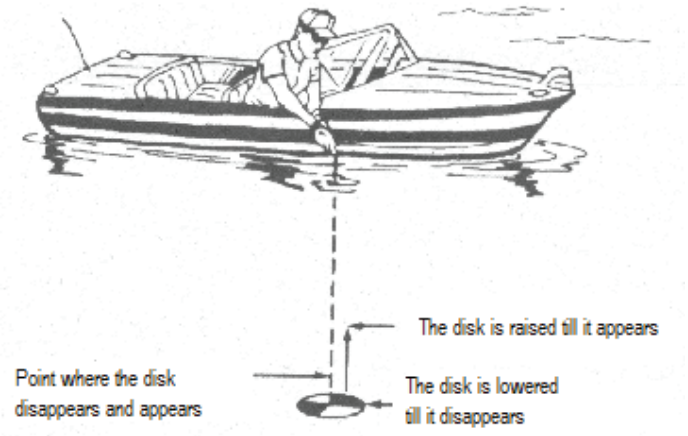

Figure 3 Illustration of how the water clarity was determined.

3.5. Bottom Depth

Bottom depth was determined using an echo sounder. This is a device used for measuring the bottom depth of the water by means of an acoustic echo. The time taken for a pulse of sound sent from the surface and returns from the bottom is calibrated in terms of the depth of water.

3.6. Current speed

A current meter dataset was as well obtained by launching a current meter in M1 at the beginning of the sampling exercise and removing it at the end of the sampling exercises. The meter was configured to correct data at an interval of five minutes. The data was then downloaded on a personal computer.

3.7. Salinity and Temperature

Salinity and Temperature were determined onsite using Hach Waterproof Conductivity Meter which is housed in a chemical resistant, dust proof, and waterproof chase. By immersing the probe at depth of about 50 cm the salinity and Temperature could be read on the screen and recorded on a waterproof pallet. This was done for all sampling sites in all the fieldwork days. The readings were to be used in assessing factors that influence high temporal variation.

3.8. Determination of Chlorophyll a

3.8.1. Material and equipments

Reagents

- Magnesium carbonate buffering solution
- 90% acetone

Materials

- Glass-fibre filter (Whatman GF/F)
- Low Vacuum (ca. 0.5 atmosphere) Filtration unit
- Glassware
- Filter holder

3.8.2. Determination of Chlorophyll-a

Suspended sediments reduce light penetration and hence lead to reduced primary productivity in the water (Mishra, 2004). Therefore, among other factors, suspended sediments influence in chlorophyll concentrations. In the algorithm development, it was assumed that the Coloured Dissolved organic

Matter is negligible. Therefore it can be deduced that in the red region of the spectrum, absorption of light is caused by water molecules and chlorophyll. To quantify this effect chlorophyll samples were collected in the field at the same locations as the suspended sediments.

Two litres of water samples were collected from the proposed sites in triplicates. A few drops of magnesium carbonates were added to the water samples before filtration to help in retention and buffer the sample since low ph causes pigment degradation (LaJollo, 1971). Due to high concentrations of suspended matter filtration process was slow. Hence, we opted to use one litre of water. Filtration was done with a low vacuum (ca. 0.5 atmosphere) to collect phytoplankton cells on a glass-fibre filter (Whatman GF/F) (Muller *et al.,* 2003[c]). Glass ware and filter holder were used for filtering. The filter was folded in half, wrapped in foil and frozen in a jar with desiccant. The chlorophyll pigment was then extracted from the phytoplankton using 2-5 ml of 90% acetone (v/v dilute with DI) (Short and Coles, 2001). Grinding was directly done in a centrifuge with a pestle for 2-3 minutes at 500 to 1000 rpm. The centrifuge tube volume was then brought to 15 ml to provide sufficient extract to fill a 10 CM spectrophotometer cell. The tube was capped to prevent evaporation and extraction was done overnight in a cool dark place. The tubes were centrifuged in a refrigerated centrifuge at 104 rpm for 10 minutes then the clear acetone supernatant was decanted into a glass tube for determination into the spectrophotometer without agitating the bottom filter pellet since the spectrophotometer is sensitive to suspended particles.

Chlorophyll-a was determined using the spectrophotometer method by measuring the absorbencies of the extract at 630nm, 647 nm, 664nm and 750nm (blank). Absorbance is the amount of light absorbed. Before taking each measurement, the spectrophotometer readings were zeroed using acetone. This was done for cell to cell blank correction Stickland and Parsons, (1968). To remove the effect of suspended sediments, the absorbencies at 630nm, 647 nm, and 664nm were corrected by subtracting it from 750nm absorbency.

Several formulas of determining chlorophyll a concentration exists (SCOR/UNESCO, (1966); Lorenzen, (1967); Stickland and Parsons, (1968); Jeffrey and Humphrey, 1975). However, the differences between the equations particularly in the calculation of chlorophyll a are negligible (<2.5%). Although all the equations below were considered, equation 4 was adopted for this study.

SCOR/UNESCO (1966): C_a (mg m^{-3}) = (11.64 D_{663} - 2.16 D_{645} - 0.1 D_{630}) v l^{-1} V^{-1}

(1)

Lorenzen (1967): C_a [$mg\ m^{-3}$] = 26.7 ($D_{663\text{-}665b}$ - $D_{663\text{-}665a}$) v l^{-1} V^{-1} **(2)**

Stickland and Parsons , (1968): C_a ($mg\ m^{-3}$) = (11.6 D_{665} - 1.31 D_{645} - 0.14 D_{630}) v l^{-1} V^{-1} **(3)**

Jeffrey and Humphrey, (1975): C_a [mg m^{-3}] = (11.85 $D_{663\text{-}665}$ - 1.54 D_{647} - 0.08 D_{630}) v l^{-1} V^{-1} **(4)**

Where D represents absorbance at the indicated wavelength, after correcting the cell-to-cell blank (in this case, the readings were zeroed using acetone) and subtracting with cell-to-cell blank of the already corrected absorbance at 750nm. $D_{663\text{-}665b}$ is the absorbance at 663-665nm read after correcting the cell-to-cell blank and subtracting the cell-to-cell blank corrected absorbance at 750nm, before acidification. In the Lorenzen (1967) formula, acidification is involved. Hence the absorbencies are read before and after the acidification. $D_{663\text{-}665a}$ represents the absorbance at 663-665nm, after correcting with the cell-to-cell blank and subtracting the cell-to-cell blank of the already corrected absorbance at 750nm, and after acidification. v stands for the volume of acetone (ml), l represents the cell (cuvette) length (cm), while V indicates the volume of filtered water (l).

An illustration of fieldwork activities is as shown in figure 4 below


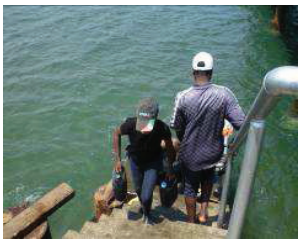


Figure 4 Illustration of the fieldwork activities

3.9. Data Preparation

Data preparation involved:

- Image selection,
- Cloud masking
- Sun glint masking

3.9.1. Image Selection

Meteosat Second Generation radiance images of channel one and channel two were retrieved from the ITC archive through the MSGDataretriever software which has the capability of calibrating the images. A total of 143 MSG images covering the in-situ sampling time were retrieved for the purpose of validation. At each of the seven pre-selected sites, three images were retrieved with a time difference of about 15 minutes to match pre-sampling, actual sampling and post sampling time. This was repeated for the seven fieldwork days. After preliminary analysis only 11 images were eventually used in this study for retrieval of the suspended sediments as shown in Table 2. This was mainly due to presence of thick cloud cover and sun glint. In addition, some images lacked data completely a cause which was not investigated.

Table 2 Meteosat Second Generation images used in this study

Date	Time
18/10/08	13:30
18/10/08	14:00
18/10/08	14:15
20/10/08	13:45
23/10/08	13:45
23/10/08	14:00
23/10/08	14:30
24/10/08	12:45
24/10/08	13:00
24/10/08	13:15
24/10/08	14:15

3.9.2. Cloud and land masking

MPEF cloud mask images for the same periods were obtained from Eumetsat data archive. These images were converted into boolean images where areas covered by water were assigned value 1 while areas covered by clouds and land were assigned value 0 (Figure 5). The Boolean images were subsequently used to mask out land and clouds from channel one and two radiance images resulting in only the radiance on the water surface.

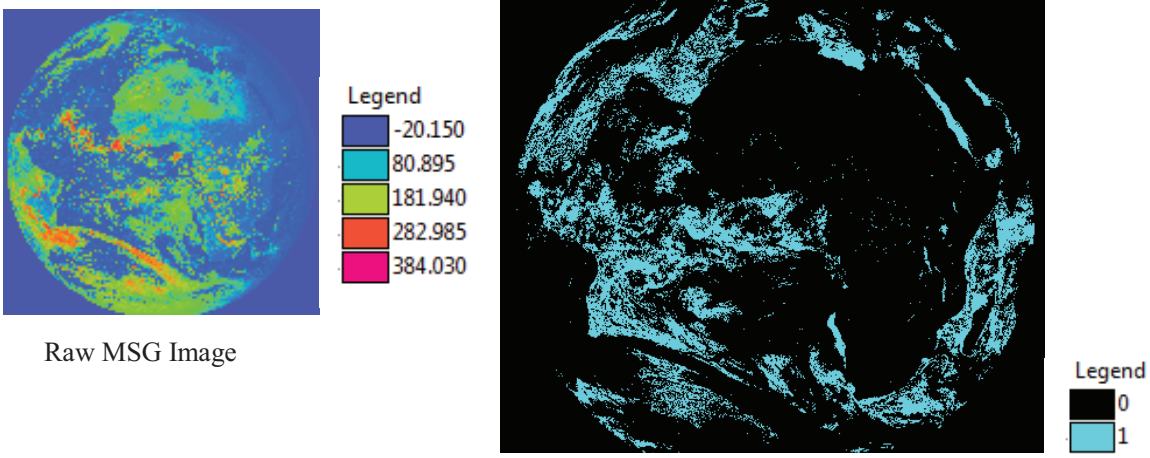

Raw MSG Image

MSG Image after Cloud Masking

Figure 5 **An example of Cloud masking product of an image taken on 18th October 2008 at 13:30 hrs GMT (0 represents land, clouds, and 0 values while 1 represents water).**

3.9.3. Sun glint masking

Sun glint effect was considered by flagging regions where the glint core angle (γ) is less than 30^0 (Brindley and Ignatov, 2006).

$$\cos\gamma = \cos\theta_v \cos\theta_s + \sin\theta_v \sin\theta_s \cos\phi_r \quad (5)$$

θ_v and θ_s, represents the satellite and sun zenith angles respectively while ϕ_r, represents the azimuth. The angles were determined using java applet. Figure 6 below shows the resultant glint core angle after applying Equation 5. The figure shows the

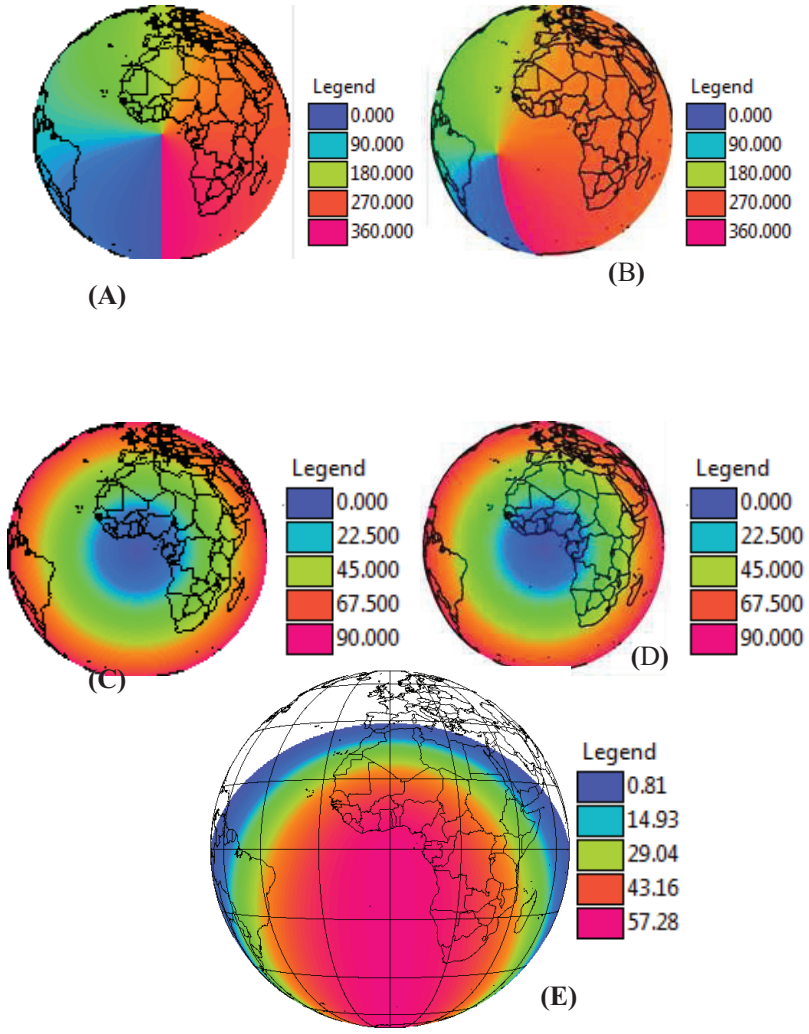

Figure 6 **Figure showing an example o the satellite azimuth (A), solar azimuth (B), satellite zenith(C), and solar zenith angles (D)and the resultant glint core angle(E) illustration for an image taken on 18th October, 2005**

4. Methodology

4.1. Introduction

The methodology adopted in this research consisted of the following steps: Deducing water leaving Radiance; normalization of water leaving radiance; calculating the exact water leaving radiance; retrieval of subsurface irradiance reflectance; and Bio-optical modeling (parameterization of inherent optical properties) and deduction of the TSS concentration.

4.2. Deducing Water leaving Radiance

Water leaving radiance is normally very small in comparison to the total light arriving at space-borne sensors. Therefore, the success of Total suspended sediments retrieval depends primarily on the accuracy of atmospheric correction algorithms (Gordon and Morel, 1983). Deker *et al* (2001) and Zhang *et al*. (1999) quantify water leaving radiance as in the range of 1 to 15% of down-welling irradiance. In this case Radiance calculated in the MSG data retriever has contributions from the water, white caps, sun glint and the atmospheric constituents (Equation 6). To achieve a reasonable water leaving radiance, one has to remove the effect of these constituents (Gordon, 1997).

$$L_t(\lambda_i) = L_{path(\lambda_i)} + T(\lambda_i)L_g(\lambda_i) + t(\lambda_i)L_{wc}(\lambda_i) + t(\lambda_i)L_w(\lambda_i) \quad \textbf{(6)}$$

Where $L_t(\lambda_{i)}$ stands for the image radiance, $L_{path(\lambda_i)}$ represents atmospheric path reflectance, $T(\lambda_i)$ is the transmittance while $L_g(\lambda_i)$ is the sun glint effect. $t(\lambda_i)$ and $L_{wc}(\lambda_i)$ are the terms expressing the diffuse transmittance, and whitecaps respectively while $L_w(\lambda_i)$ represents the water leaving reflectance.

In this case only the path radiance was taken into account. This was because MSG data has a low resolution hence the white caps effect was assumed to have been taken care of by averaging which is as a result of large pixel size (Gordon, 1997). The sun glint was as well masked hence also not considered in the atmospheric correction and Equation 5 becomes:

$$L_t(\lambda_{i)} = L_{path(\lambda_i)} + t(\lambda_i)L_w(\lambda_i) \quad \textbf{(7)}$$

The path radiance which represents contributions of air molecules and aerosol effects was calculated using 6s model (Vermote, *et al.,* 1997). However, the results from 6s were in form of reflectance. Therefore to convert the path reflectance to radiance the following expression was used (Gordon, 1997) which relates reflectance with radiance L

$$\rho = \frac{\pi L}{F_0 \cos\theta_0} \quad \textbf{(8)}$$

Making L the subject of the formula results into

$$L = \frac{\rho F_0 \cos\theta_0}{\pi} \quad \textbf{(9)}$$

Where F_0 refer to the extraterrestrial whereas θ_0 is the solar zenith angle (the angle between the line from the point on the sea surface and the examination to the sun and to the local vertical). The θ_0 is equal to 46 hence Cos 46 is equal to 0.984 which is approximately 1.

With path radiance known ($L_{path(\lambda_i)}$) rearranging Equation 7 making water leaving radiance term ($t(\lambda_i)L_w(\lambda_i)$) the subject of the formula, results into;

$$t(\lambda_i)L_w(\lambda_i) \quad = L_t(\lambda i) - L_{path(\lambda_i)} \quad \textbf{(10)}$$

To compute the path radiance, the following steps were followed in 6s.

Geometric conditions

In geometrical conditions, user's option was chosen. This is because this option allows one to specify the temporal aspect as well as the illumination angulations which are vital in this study. This is due to the dependence of the water leaving reflectance and thus the inherent optical properties on the radiometric conditions (Mobley, 1994; Muller, 2003[b]). Month and day as well as solar zenith, solar azimuth, sensor zenith and sensor azimuth angles were input. These angles were determined using an executable file developed by 52-North initiative. The angles used were as shown in table 3. It should be noted that the angulations are only valid for the specified location at a specified time, thus they were entered corresponding to the time and site of the validation dataset.

Table 3 Table showing the illumination angulations

Date	**Station**	**satellite Zenith angle (Degrees)**	**satellite azimuth angle (Degrees)**	**Sun Zenith angle (Degrees)**	Sun azimuth angle (Degrees)
18/10/08:1330	m1	46.246	273.604	46.246	261.057
18/10/08:1400	m2	46.242	273.571	46.246	260.969
18/10/08:1415	sm	46.242	273.571	46.246	260.553
20/10/08:1345	m1	46.246	273.604	46.246	260.668
23/10/08:1345	m1	46.246	273.604	46.246	257.135
23/10/08:1400	m1	46.246	273.604	46.246	257.135
23/10/08:1430	m2	46.242	273.571	46.246	259.056
24/10/08:1245	m1	46.246	273.604	46.246	258.284
24/10/08:1315	m1	46.246	273.604	46.246	258.284
24/10/08:1300	m1	46.246	273.604	46.246	258.284
24/10/08:1415	m2	46.242	273.571	46.246	258.267

Atmospheric model

Under the atmospheric model, tropical atmospheric profile was chosen because the validation site was in a tropical environment. Maritime aerosol model was used because the correction was over marine environment.

Visibility

A visibility of 10km was used in accordance to ground station measurements at the sampling time. The data was sourced from weather data archive freely supplied on the internet from; http://www.wunderground.com/history/airport/HKMO/2008/10/25/DailyHistory.html website.

Target and sensor altitude

Target and sensor altitude were selected as sea level (because the validation site was at the sea water) and satellite level respectively.

Spectral conditions

Spectral conditions were selected as step by step output with the filter function=1 while the bands were selected as Meteosat (0.350-1.110). This band is large enough (0.35-1.10 μm*)* to include both scattering effects and water vapor. The error related to this approximation is smaller than one percent. Thus it was considered appropriate for this study.

Wavelength information

Absorption Wavelength info(micron) and Wavelength sup(micron) for channel one were taken to be minimum and maximum of the band width; 0.56-0.74 and 0.74-0.88 for channel one and two respectively.

Ground Reflectance Type

Water surface was assumed to be uniform in this study due to the averaging caused by the large pixel size (Gordon, 1997). Thus ground reflectance type was chosen as homogeneous surface with no directional effects. The surface reflectance specification was mean spectral value of clear water. Atmospheric correction mode was chosen with Lambertian surface assumption.

The results obtained after running the 6s model are as shown in the table 4.

Table 4 Table showing 6s model results

Date & Time	**18/10/08 :1330**	**18/10/08 :1400**	**18/10/08 :1415**	**20/10/08 :1345**	**23/10/08 :1345**	**23/10/08 :1400**	**23/10/08 :1430**	**24/10/08 :1245**	**24/10/08 :1315**	**24/10/08 :1300**	**24/10/08 :1415**
Station	m1	m2	sm	m1	m1	m1	m2	m1	m1	m1	m2
PR in channel 1	0.107	0.107	0.107	0.104	0.106	0.106	0.105	0.105	0.105	0.105	0.105
PR channel 2	0.073	0.073	0.074	0.073	0.074	0.074	0.073	0.073	0.073	0.073	0.073
Tau	0.05866	0.0586	0.0586	0.0586	0.0586	0.0586	0.0586	0.0586	0.0586	0.0586	0.0586
Channel 1		6	6	6	6	6	6	6	6	6	6
Tau channel 2	0.0213	0.0213	0.0213	0.0213	0.0213	0.0213	0.0213	0.0213	0.0213	0.0213	0.0213
Julian day	292	292	292	294	297	297	297	298	298	298	298

PR= Intrinsic atmospheric reflectance; Tau= Rayleigh Optical Thickness

4.3. Normalization of water leaving radiance

The normalization of Water Leaving Radiance in equation 10 ($t(\lambda_i)L_W(\lambda_i)$) which include transmittance was necessary so as to also account for the variations in solar zenith angle, and earth-sun distance. The Equation 11 was used (Gordon and Clark, 1981).

$$L_{WN}(\lambda) = \frac{L_W(\lambda)}{t(\lambda,\theta_0)\cos\theta_0\left(\frac{d_0}{d}\right)^2} \quad \textbf{(11)}$$

Where $t(\lambda,\theta_0)$ stands for diffuse atmospheric transmittance and $\frac{d_0}{d}$ the ratio of the mean and actual earth-sun distance.

$t(\lambda, \theta o)$ was calculated through the following equation (Penndorf, 1957)

$$t(\lambda,\theta_0) = e^{\frac{\frac{1}{2}\tau_R(\lambda)+\tau_{0_3}(\lambda)}{\cos\theta_0}} \quad \textbf{(12)}$$

Where τ_R stands for Rayleigh optical thickness while τ_{0_3} represents Ozone optical thickness

$\frac{d_0}{d}$ are equal to:

$$\frac{d_0}{d} = 1 + 0.0167\cos\left[\frac{2\pi(J-3)}{365}\right] \quad \textbf{(13)}$$

J represents the Julian day of the year.

Figure 7 below shows an example of Water Leaving Radiance and the resultant Normalized Water leaving Radiance of channel 2 of an image taken 0n 18th October, 2008 at 13:30 hrs GMT expressed as a percentage.

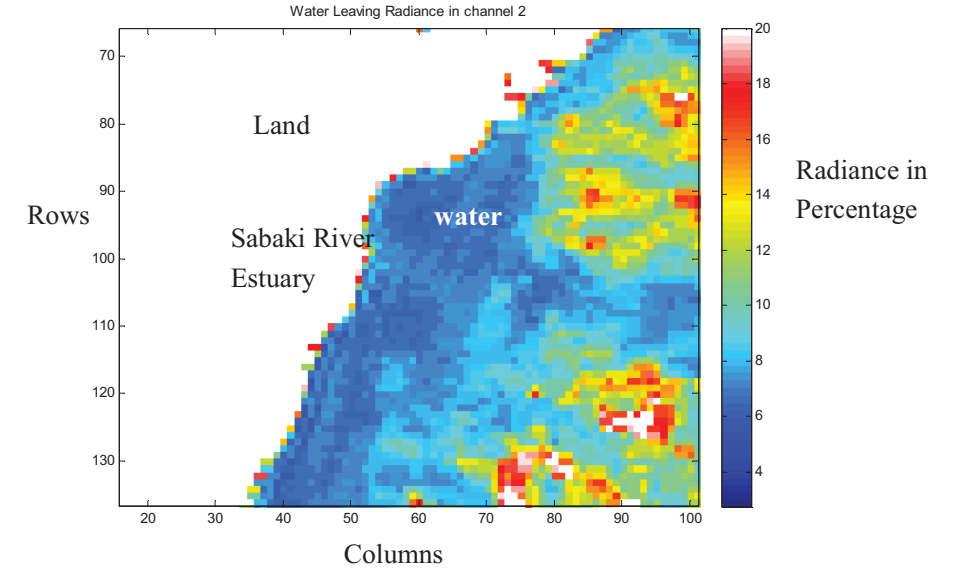

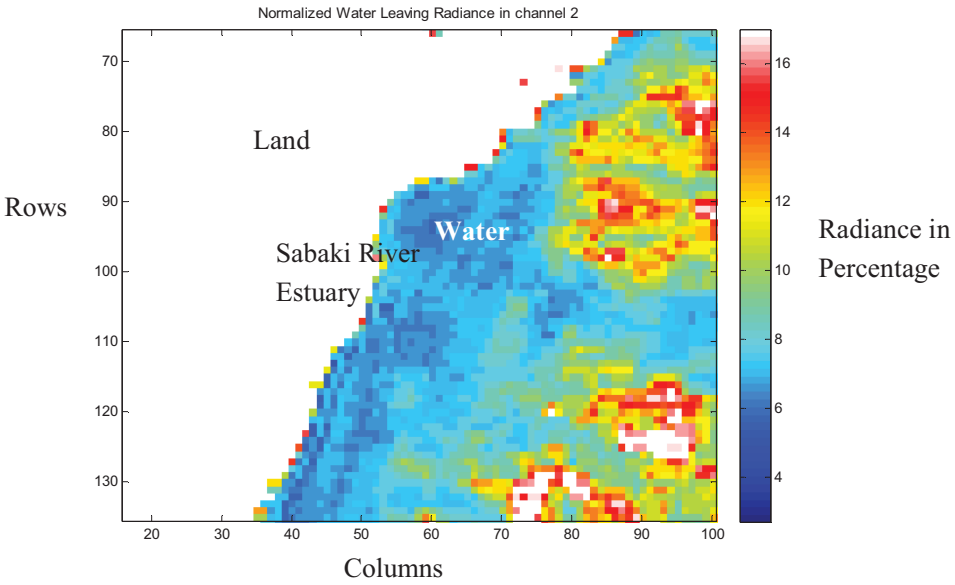

Figure 7 **Figure showing Water Leaving Radiance (A) and Normalized Water Leaving Radiance (B) of channel 2 of an image taken on 18th October 2008 at 13:30 hrs GMT**

4.4. Calculating the Exact Water Leaving Radiance

To calculate Exact Water Leaving Radiance the Normalized Water Leaving Radiance (Equation 10) was corrected for bidirectional effects (dependencies on geometry).

Considering that equation 11 can be rewritten as equation 14 below (Muller *et al.,* 2003[c]*)*:

$$L^{S}WN(\lambda,\theta,\phi) = \frac{L^{S}W(\lambda,\theta,\phi,\theta_0,\tau_a,W,Chl)}{t(\lambda,\theta_{0,})\cos\theta_0\left(\frac{do}{d}\right)}$$

(14)

The dependencies of the above expression with respect to geometry (viewing and solar angles), as well as with respect to the Inherent Optical Properties i.e. λ (wavelength) and *Chl*(chlorophyll) can be expressed as equation 15 below (Muller *et al.,* 2003*)*:

$$L_W(\lambda,\theta,\phi,\theta_0,\tau_a,Chl) = E_d(0^+,\lambda,\theta_0,\tau_a)R(\theta',W)\frac{f(\lambda,\theta_0,\tau_a,Chl)}{Q(\lambda,\theta',\phi,\theta_0,\tau_a,Chl)}\frac{b_b(\lambda,Chl)}{a(\lambda,Chl)}$$

(15)

Where E_d is Above water downward irradiance; $R(\theta',W)$ is the reflection- refraction term. The quantities expressed in $L^{S}_{WN}(\lambda,\theta,\phi)$ (Normalized Water Leaving Radiance) retain strong bidirectional nature that can be seen by substituting equation 15 for the numerator on the right hand side of equation 14. These dependencies make comparisons for normalized water leaving Radiances pixel to pixel of the scene and from one day to another not possible. To solve this problem assumption is that the sun was at zenith and that the pixel has been seen vertically enables exact normalized water leaving radiance to be determined that no longer depends on bidirectional factors. To transform the $L^{S}_{WN}(\lambda,\theta,\phi)$ to $L^{ex}_{WN}(\lambda,\theta,\phi)$ a ratio is computed as shown below.

$$\frac{L^{ex}_{WN}(\lambda)}{L^{S}WN(\lambda)} = \frac{E_{d(0^+,\lambda,\theta_0)}L_W[\lambda,0,0,0,\tau_a,W,Chl]}{E_d(0^+,\lambda,0)L^{S}W[\lambda,\theta,\phi,\theta_0,\tau_a,W,Chl]}$$

(16)

where $E_{d(0^+,\lambda,\theta_0)}$ and $L_W[\lambda,0,0,0,\tau_a,W,Chl]$ represent incident irradiance and water-leaving radiance respectively that are unknown and are determined for θ o = θ′ = θ = 0 and φ, although indeterminate, is denoted also as φ = 0.

When Equation (equation 15) is used to expand the terms $L_W[\lambda,0,0,0,\tau_a,W,Chl]$ and $L^S{}_W[\lambda,\theta,\phi,\theta_0,\tau_a,W,Chl]$ in (Equation 16), the solution obtained is:

$$L^{ex}{}_{WN} = L^S{}_{WN}(\lambda,\theta,\phi)\frac{R_O}{R(\theta^{'}W)}\frac{f_O(\lambda,\tau_a,Chl)}{Q_O(\lambda,\tau_a,Chl)}\left(\frac{f(\lambda,\theta_O,\tau_a,Chl)}{Q(\lambda,\theta^{'},\phi,\theta_O,\tau_a,Chl)}\right)^{-1} \quad \textbf{(17)}$$

R_O and R (θ′,W) ratio is the reflection- refraction term while fo(λ,τa,Chl) is the value of the function f when θo = 0 as a function of wavelength (λ), aerosol optical thickness(τa) and chlorophyll(Chl) . Qo (λ, τa, Chl) is the value of the function Q when θo = 0 and θ = θ′ = 0 (Morel and Gentili 1996). In this case, Equation 17 was used to determine the exact water leaving radiance where Q was taken to be 3.75 and Qo was taken to be 3.5 according to simulations done in by (Morel and Gentili, 1996). Figure 8 below shows an example of the Exact Water Leaving Radiance of channel 2 of an image taken on 18th October, 2008 at 13:30 hrs GMT.

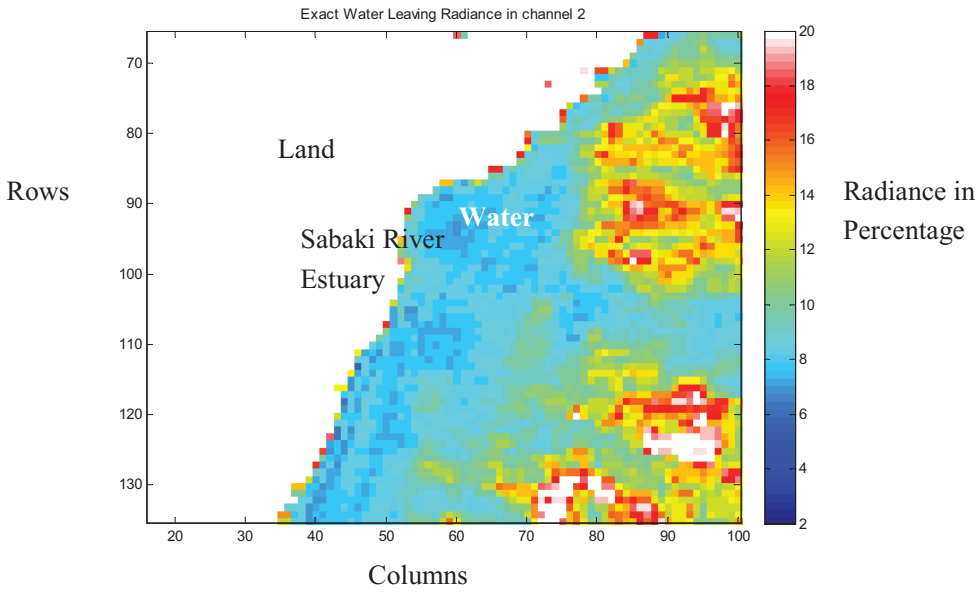

Figure 8 **Figure showing Exact Normalized Water Leaving Radiance of Channel 2 of an image taken on 18th October 2008 at 13:30 hrs GMT**

4.5. Retrieval of subsurface irradiance reflectance

The irradiance reflectance (Equation 18) has been extensively determined at sea, and also has been modeled. As only irradiances are involved in its definition, its only angular dependencies are related to the illumination geometry, through the factor $f(\lambda, \theta_0, \tau_a, Chl)$ in equation (19). The irradiance reflectance and the exact normalized water-leaving radiance are related through Equations (20) and (15) as equation 21 (Muller, *et al.,* 2003).

$$R(0^-, \lambda) = \frac{E_u(0^-, \lambda)}{E_d(0^-, \lambda)} \quad \textbf{(18)}$$

$$R(0^-, \lambda) = f(\lambda) \frac{b_b(\lambda)}{a(\lambda)} \quad \textbf{(19)}$$

$$L^{ex}WN\ (\lambda) = \frac{R(0^-, \lambda, \theta_0)\overline{F_0}(\lambda)R_0}{Q_n(\lambda, \theta, \tau_a, Chl\ )} \quad \textbf{(20)}$$

$\overline{F_0}$ ……represents the extraterrestrial solar irradiance.

$$R(0^-, \lambda, \theta_0) = \frac{L^{ex}WN(\lambda)(Q_n(\lambda, \theta, \tau_a, Chl))}{\overline{F_0}(\lambda)R_0} \quad \textbf{(21)}$$

The figure 9 shows an example of the subsurface irradiance reflectance of channel 2 retrieved from an image acquired on 18th October 2008 at 13:30 hrs GMT. At this stage the subsurface irradiance was used for bio-optical modelling.

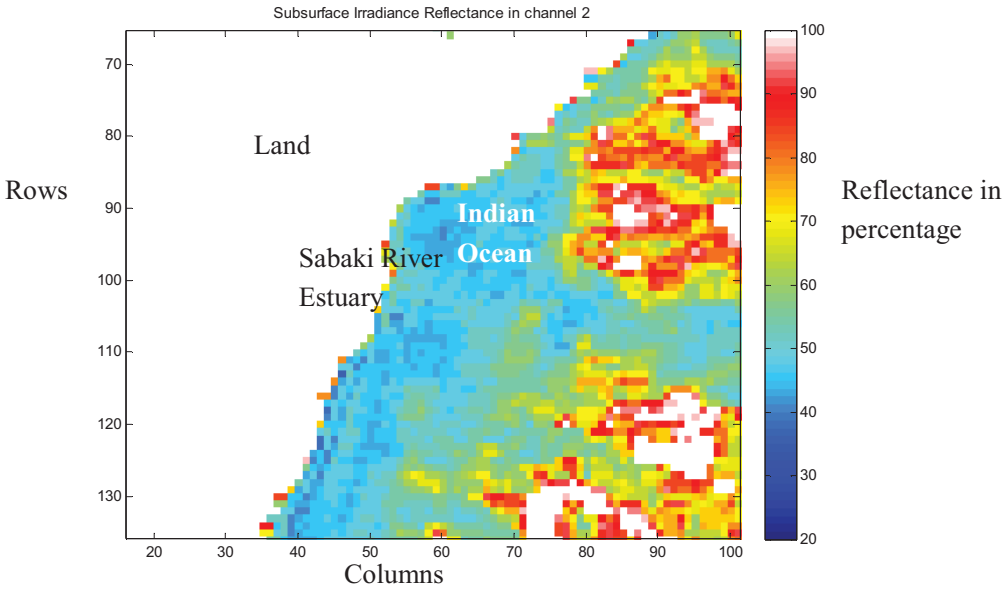

Figure 9 **Figure showing Subsurface Irradiance Reflectance of Channel 2 of an image taken on 18th October 2008 at 13:30 hrs GMT**

4.6. Bio-optical modelling

The total subsurface irradiance reflected from the water surface is a combination of all the optically important water constituents namely chlorophyll, colored dissolved organic matter and total suspended sediments. This necessitated Parametization in order to get the back scattering which was used in this study to compute concentration of the total suspended sediments concentration. Equation 22 (Gordon *et al.,* 1988) and Equation 24 (Morel and Prieur, 1977); and Equation 26 (Gordon, *et al.,* 1975) were used to relate the inherent optical properties to the subsurface irradiance reflectance. However, only Equation 22 and 24 were presented in the results. This was because the Gordon, *et al.,* (1975) model gave negative results due to higher value of backscattering as compared to absorption (Muller *et al*, 2003).

4.6.1.1. Parametization

4.6.1.1.1. Parametization of backscattering using Gordon *et al.,* (1988) model

Inherent optical properties of the two SEVIRI visible bands namely channel one which is centered at 0.635 μ m and channel 2 which is centered at 0.81 μ m were parameterized. Assuming that in channel 2, absorption is only caused by water, backscattering was computed by rewriting equation 22 as shown in Equation 23.

Equation 21 represents the Gordon *et al.,* (1988).

$$\frac{R(0^{-},\lambda,\theta_0)}{Q} = l_1 \frac{b_b}{a} \quad \textbf{(22)}$$

Where l_1 is taken to be equal to 0.0949 (Gordon *et al.,* 1988). Q is the ratio of upwelling radiance to the upwelling irradiance. a represents the absorption coefficient , b_b stands for the backscattering while $R(0^{-},\lambda,\theta_0)$ represents the subsurface irradiance reflectance.

$$b_b = \frac{aR\ (0^{-},\lambda,\theta_0)}{l_1 Q} \quad \textbf{(23)}$$

4.6.1.1.2. Parametization of backscattering using Morel and Prieur, (1977) model

Equation 24 represents Morel and Prieur, (1977) model.

$$R(0^{-},\lambda,\theta_0) = f \frac{b_b}{a} \quad \textbf{(24)}$$

f was considered to be constant at 0.33 as determined by (Morel and Prieur, 1977).

To parameterize backscattering Equation 24 was rewritten as shown in equation 25.

$$b_b = \frac{aR\ (0^-, \lambda, \theta_0)}{f}$$

(25)

4.6.1.1.3. Parametization of backscattering using Gordon, *et al.,* (1975) model

$$R(0^-, \lambda, \theta_0) = f' \frac{b_b}{a + b_b}$$

(26)

f' was as well considered to be constant at 0.33 in this case.

To parameterize backscattering, Equation 26 was rewritten as shown in equation 27.

$$b_b = \frac{aR\ (0^-, \lambda, \theta_0)}{R\ (0^-, \lambda, \theta_0) - f'}$$

(27)

4.6.1.2. Extrapolation of the backscattering in channel two to channel one

For extrapolation purposes, Maritorena et al., (2002) equation was applied where the backscattering coefficients in Equation 23 and Equation 25 and Equation 27 were independently substituted in equation 28 as shown in equation 29.

$$b_{bp}(\lambda) = b_{bp}(\lambda_0)(\frac{\lambda_0}{\lambda})^{-\eta}$$

(28)

$$b_{bchannel\ 1} = b_{bchannel\ 2}\left(\frac{810}{635}\right)^{-\eta}$$

(29)

$-\eta$ This represents the power-law exponent for particulate backscattering coefficient. This coefficient was assumed to be equal to 1.7 for the large particles and 0.3 for the small

particles during the computation in this study (Morel, 1974).

4.6.2. Retrieval of TSS from Back Scattering

After computing the backscattering of the suspended sediments, retrieval of the concentrations of suspended sediments was done using equation 30 (Albert and Gege, 2006) as shown in Figure 10.

$$b_b(\lambda) = 1/2b_w(\lambda) + b_b x^* C_x \quad \textbf{(30)}$$

$b_b x^*$ represents the specific backscattering coefficient of suspended sediments. The backscattering coefficient is wavelength independent and is equivalent to 0.0086m^2/g.

C_x represents the suspended sediments concentrations.

Equation 30 above can be rewritten as:

$$C_x = \frac{b_b(\lambda) - 1/2b_w}{b_b x^*} \quad \textbf{(31)}$$

b_w Value refers to the backscattering caused by water molecules.

In this case it was considered as equivalent to 0.00105 and 0.00040 at 635 and 810 nm wavelengths respectively as calculated in Smith and Braker, (1981).

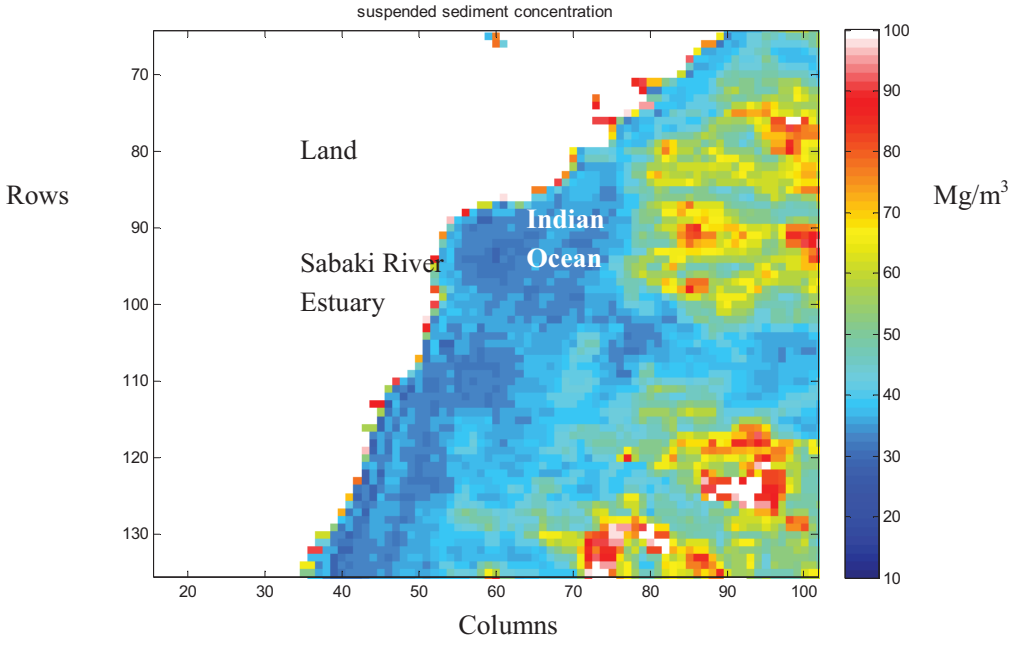

Figure 10 **An example of the TSS concentration levels in (mg/m^3) for a part of the globe processed using MSG TSS CODE from an image taken on 18th October, 2008 at 13:30 hours (GMT time).**

4.7. MSG TSS CODE

An algorithm[Θ] was designed for MSG channel one and two (visible bands) only. The procedure designed involved conversion of the path reflectance to Radiance, correction of the MSG images of channel one and two to get the water leaving radiance; calculating the Normalised Water Leaving Radiance; calculating the Exact Normalised water leaving radiance; retrieval of the subsurface irradiance reflectance; Parametization of backscattering and retrieval of the total suspended sediments. These steps are explained in detail in the above section. The constants used are as shown in table 5 below (see Appendix 5).

Table 5 Table showing the constants used in the designed algorithm

symbol	Value	units	source	description
cos_tts	0.984807753	-		cos of sun zenith angle
J	292	-	Julian calender	Julian day
do_d	1 + 0.0167*cos((2*pi*(J -3)) / 365);	-	Muller, 2003[b].	ratio of mean and actual earth-sun distance
wl_	[635, 810];	nm	ESA, 2004	wavelength
a_	0.107 (1) 0.073 (2)	Percentage	6s model	atmospheric contribution to measured radiance (635,810)
tau_R_	0.05866(1) 0.02130(2)		6s model	Rayleigh optical thickness (635,810)
tau_03_	[0.00000(1) 0.00000](2)	-	Assumed to Be zero (Gordon, 1997)	Ozone optical thickness, (We assume it has no effect)
R_0_	0.529(1) 0.529(2)	-	Morel and Gentili 1996	Reflection
R_	0.460(1) 0.460(2)		Morel and Gentili 1996	Refraction
f_0_	0.33(1) 0.33(2)	-	Morel and Gentili 1996	scattering contribution of sun angle=0
Q_0_	3.5(1) 3.5(2)	-	Morel and Gentili 1996	scattering contribution of sun angle=0
f_Q_	0.092(1) 0.092(2)	-	Morel and Gentili 1996	ratio of scattering contribution
Q_n_	3.75(1) 3.75(2)	-	Morel and Gentili 1996	Ratio of irradiance to any (direct / diffuse) radiance
F_0_mean_	1.8(1) 1.2(2)		Nickel & labs 1984	Extra terrestrial solar irradiance
bsw_(1) bsw_(2)	0.00105(1) 0.00040(2)	m^{-1}	Mobley, 1994	backscattering of seawater
bbx_	0.0086 8.6	M^2/g M^2 /mg	Albert and Gege, 2006	specific backscattering coefficient of suspended matter
f_Q_0_(1)	f_0_(1) / Q_0_(1);	-	Morel and Gentili 1996	ratio of scattering contribution at sun angle=0
f_Q_0_(2)	f_0_(2) / Q_0_(2)	-	Morel and Gentili 1996	ratio of scattering contribution at sun

Θ Used in this case to mean: a step-by-step problem-solving procedure or to be precise: a computational procedure for solving a problem in a finite number of steps".

				angle=0
l_	0.0949	-	Gordon, 1988	parameter related to the geometry
a_h20_	0.324(1) 2.070(2)		Smith and Baker, 1981	light absorption of water
chl_	0.001500(1) 0.000(2)		Field work Assumed to be Zero	light absorption of chlorophyll
a_tot_	a_h20_ + a_chl_			total light absorption
cx	Equation	g/m^3 or mg/m^3		TSS Concentration

- means unitless

5. Results

5.1.1. Results of Total Suspended Sediments Field Data Analysis

The total suspended sediments concentrations which were determined in the laboratory for 147 water samples collected during the fieldwork at Sabaki Estuary (see section 3.1 for details) were analyzed. The suspended sediments concentrations ranged from 24.3 to 52.7 mg/l with a mean of 31.11 and a standard deviation of 5.17. The graph below (figure 11) represents the means as well as the minimum and the maximum concentrations per day. A statistical test indicated significant difference in the means of the total suspended sediments concentration, bottom depth and Secchi disk depth during springtide and neaptide (One-sample t-test, where, df = 20 and P = 0.001 for TSS, df = 20 and P < 0.001 for bottom depth, df = 20 and P < 0.001 for Secchi disk depth) (see appendix 4). The actual values are presented in appendix 1.

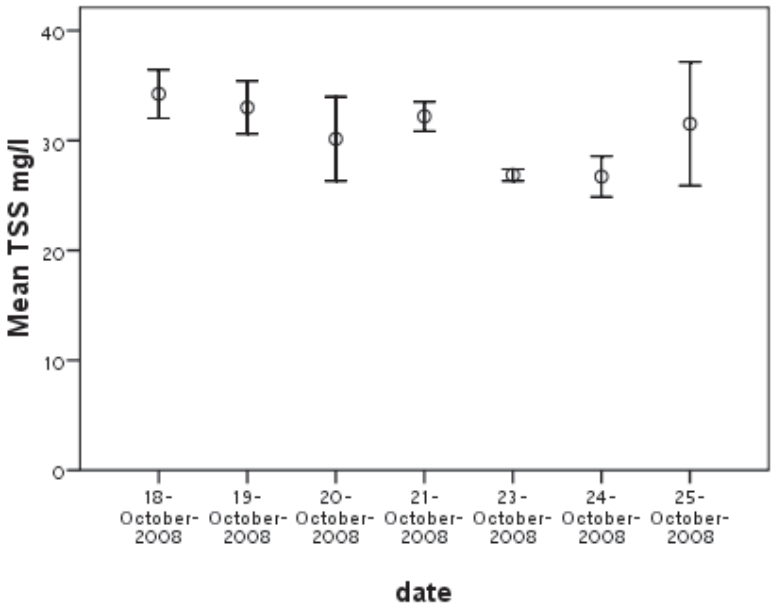

Figure 11 **Graph representing the means as well as the minimum and the maximum concentrations per day throughout the study period (18th-25th October 2008).**

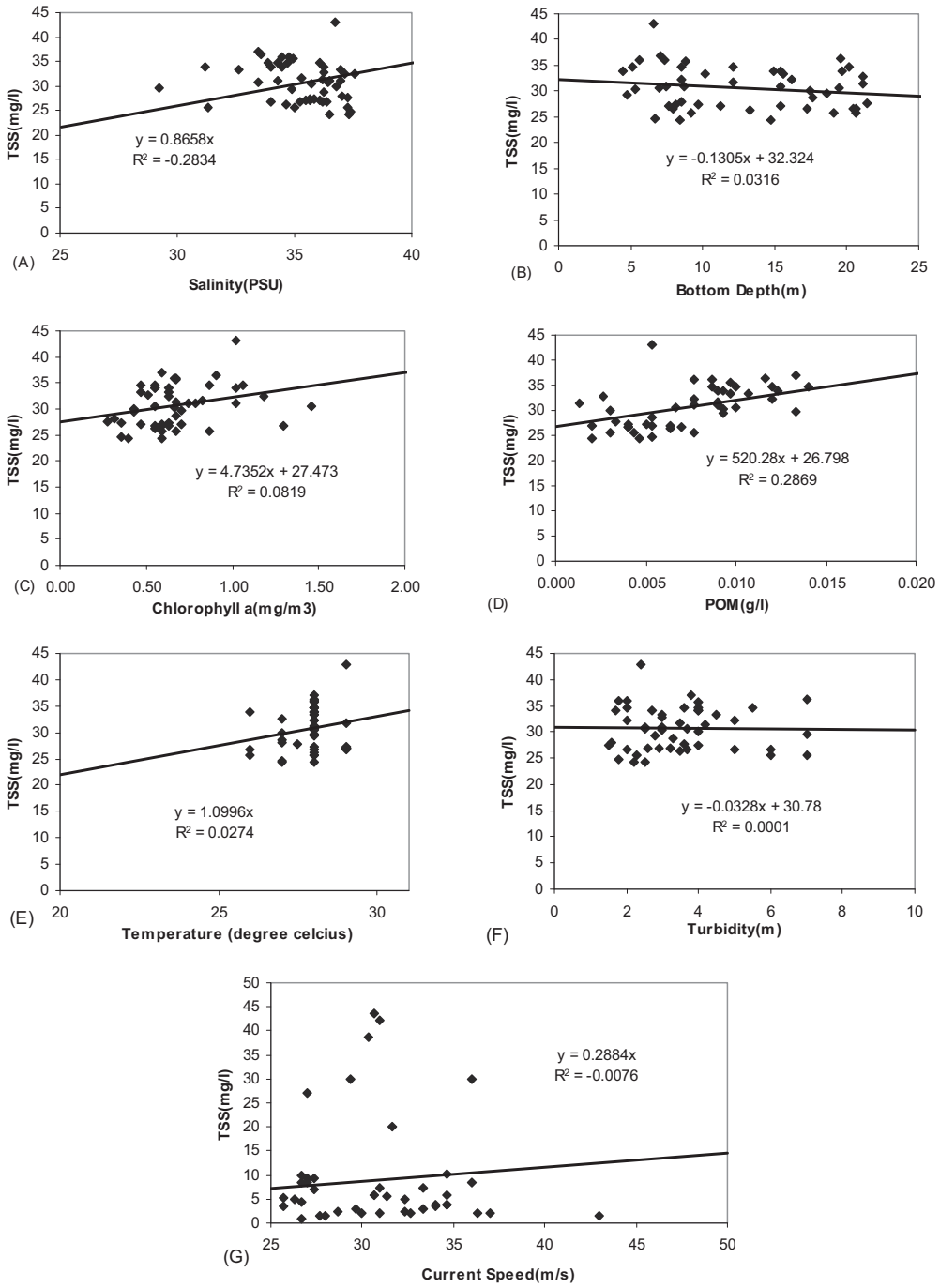

Figure 12 **Scatter plots of the relationship between TSS and Turbidity, Bottom Depth, Chl-a, Salinity, Particulate organic matter, temperature and current speed**

Table 6 **Table showing the relationship between measured TSS concentration and Turbidity, Bottom Depth, Chl-a, Salinity, Particulate organic matter, temperature and current speed**

Parameter Related to TSS (mg/l)	*Correlation Coefficient*	*coefficients and Intercept of Regression*	*Regression Analysis(R^2)*
Secchi Disk/Turbidity(m)	-0.012	y = -0.0328x + 30.78	0.0001
Bottom Depth(m)	-0.178	y = 520.28x + 26.798	0.2869
chla(mg/m3)	0.286	y = 4.7352x + 27.473	0.0819
Salinity (PSU)	-0.198	y = 0.8658x	-0.2834
POM(g/l)	0.536	y = 520.28x + 26.798	0.2869
Temperature(Degrees Celsius)	0.167	y = 1.0996x	0.0274
Current Speed(m/s)	0.016	y = 0.2884x	-0.0076

The analysis of the insitu data of the validation site has been presented in figure 12, A to G. The statistical analysis is presented in Table 6. TSS concentration and Secchi disk Depth shows a negative correlation of -0.01 while the R^2 was found to be zero indicating that there was no relationship between the concentration of TSS and the turbidity during the period of study. The relationship between bottom depth and TSS Concentration indicate a negative relationship of -0.178 and an R^2 of 28.7% which quite high as compared to turbidity. Chlorophyll a and TSS concentration related so positively with a correlation of 0.286 and an R^2 of 8.19% which is greater than turbidity relation but lower than that of chlorophyll. The correlation between TSS concentration and salinity was negative at -0.198 while the R^2 was 28.3% which the largest negative R2 in all the related parameters considered during the study period. The correlation coefficient of TSS concentration verses the Particulate Organic Matter was the highest at 0.536 while the R^2 was 28.7 %. Temperature and TSS concentration related positively with a correlation coefficient of 0.167 and an R^2 of 2.74%. Details of the corresponding Equations of all the parameters which were related in this study are shown in table 6 above.

5.1.2. MSG TSS Modelled Results

The MSG TSS CODE developed on a Matlab platform, as part of this study, was used to analyse the 11 MSG images that satisfied the condition necessary for extraction of the suspended sediments (see section 2.1). The CODE has the capability of processing the whole Globe MSG images. Figure 13 shows an example of the TSS concentration levels for a part of the globe processed from an image taken on 18th October, 2008 at 13:30 hours (GMT time). The red colour indicates high TSS concentrations whereas the blue colour shows areas with low concentrations levels. From the results it is evident that the developed code has the capability of detecting and extracting TSS concentrations. However, the deduced processing parameters were localised, along the Kenyan Coast in particular

Sabaki River Estuary, (validation site also referred as study area). The extraction of the TSS concentrations was done for small and large particles separately using Gordon et al (1988) and Morel and Prieur (1977) model. The results are as shown in table 7 and 8 below.

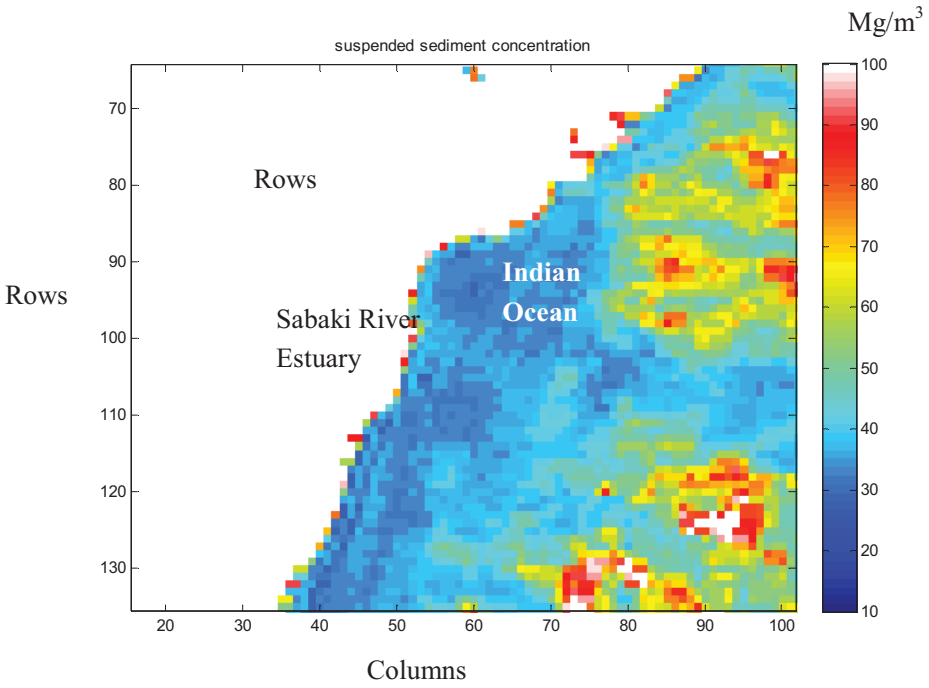

Figure 13 **An example of the TSS concentration levels in (mg/m^3) for a part of the globe processed using MSG TSS CODE from an image taken on 18th October, 2008 at 13:30 hours (GMT time).**

Table 7 **Extracted and measured TSS concentrations for Large and Small particles using Gordon et al 1988 model**

Date	*station*	*Modelled TSS conc. (Small particles)*	*Modeled TSS Conc. (Large particles)*	*measured TSS Conc*
18/10/08:1330	m1	29.4309	41.3809	34.667
18/10/08:1400	M2	31.4023	44.1527	37.000
18/10/08:1415	sm	31.4004	44.15	35.667
20/10/08:1345	m1	33.3736	46.9218	38.000
23/10/08:1345	m1	31.4004	44.1527	33.000
23/10/08:1400	m1	29.429	41.3809	33.000
23/10/08:1430	m2	23.5169	33.0656	27.000
24/10/08:1245	m1	25.4882	35.8374	25.667
24/10/08:1315	m1	27.4596	38.6091	25.667
24/10/08:1300	m1	25.4882	35.8374	25.667
24/10/08:1415	m2	21.5456	30.2938	23.333

Table 8 **Extracted and measured TSS concentrations for Large and Small particles using Morel and Prieur (1977) model**

Date	*station*	*Modelled TSS conc. (Small particles) (mg/m^3)*	*Modeled TSS Conc. (Large particles) (mg/m^3)*	*measured TSS Conc(mg/l)*
18/10/08:1330	m1	31.7386	44.6256	34.667
18/10/08:1400	M2	33.8645	47.6147	37.000
18/10/08:1415	sm	33.8624	47.6118	35.667
20/10/08:1345	m1	35.9904	50.5759	38.000
23/10/08:1345	m1	33.8163	47.5469	33.000
23/10/08:1400	m1	31.6933	44.5619	33.000
23/10/08:1430	m2	25.3263	35.6097	27.000
24/10/08:1245	m1	27.442	38.5844	25.667
24/10/08:1315	m1	29.5644	41.5686	25.667
24/10/08:1300	m1	27.442	38.5844	25.667
24/10/08:1415	m2	23.1971	32.6159	23.333

5.1.3. Validation

5.1.3.1. Validation of Gordon *et al.,* 1(988) model Results

The validation included a comparison of the TSS concentrations extracted using MSG TSS CODE with the TSS lab measurements. A scatter plot of the TSS concentration versus the TSS lab measurements for small particles showed a distinct difference between the neaptide and springtide which was depicted by two clusters. A regression analysis result was 85%, correlation coefficient (r) was observed to be 0.92 (Figure 14 (a)), while the absolute Root Mean Square Error was 3.44 mg/m^3. A comparison of the large particles with MSG TSS CODE results indicated the same correlation coefficient of 0.92 (Figure 14 (b)) while the the Root Mean Square Error was 2.73mg/m^3.

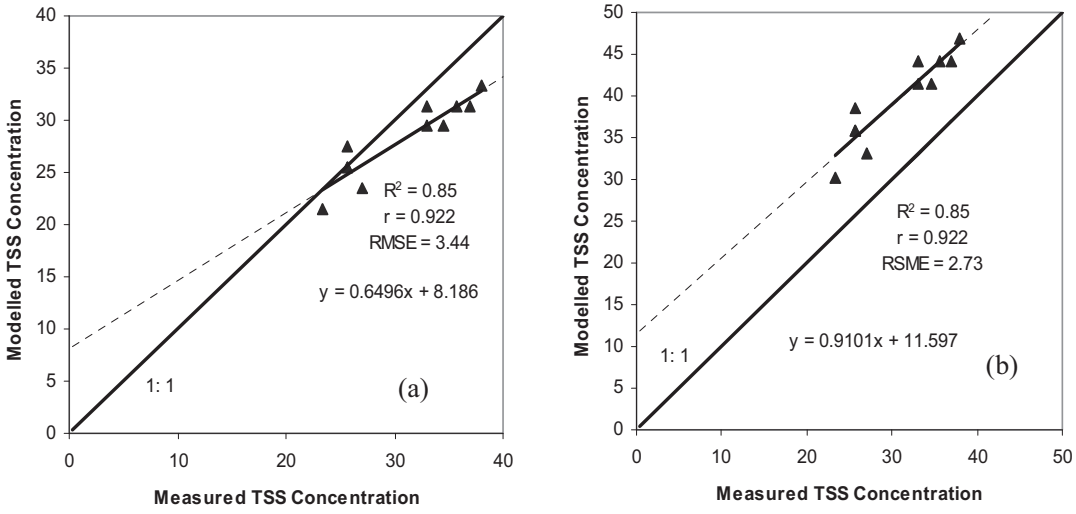

Figure 14 **Scatter plot of the relationship between modelled and measured TSS concentrations for Small Particles (a) and Large Particles (b).**

5.1.3.2. Validation of Morel and Prieur (1977) model Results

Regression analysis of Morel and Prieur, (1977) model results was 85%, correlation coefficient (r) was observed to be 0.92 (Figure 15 (a)and (b)) for both large and small particles. The absolute Root Mean Square Error differed with small particles having 2.81 mg/m^3 while the large particles had 12.08 mg/m^3.

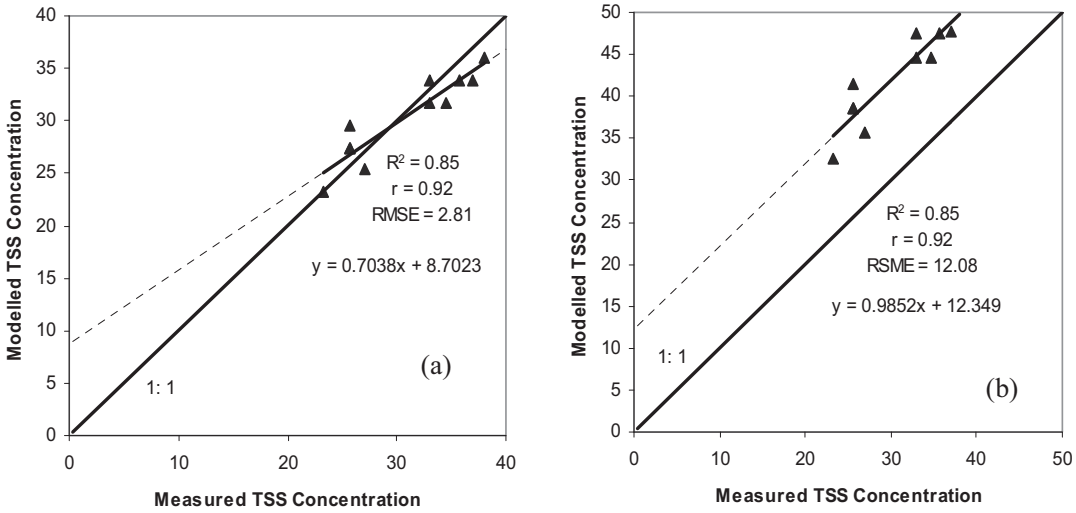

Figure 15 **Scatter plot of the relationship between modeled and measured TSS concentrations for Small Particles (a) and Large Particles (b).**

5.1.4. Spatio-Temporal Variations

For a spatio-temporal assessment of the sediment concentration along the Kenyan Coast, TSS concentrations were retrieved from available good quality MSG images at intervals of 15 minutes for the period between 18 and 24 October. The retrieved data sets were plotted on a line graph and the results are presented in Fig 16. The results indicate three distinct trends of changes in TSS concentration: 1) marked low concentration for locations M1, M2 and M3, (sites close to the land)with M2 exhibiting higher concentration than M1 and M3 due to its proximity to the river mouth; 2) an increasing sediment concentration seawards i.e. further from the land as shown by sites M4 and M6; and 3) an anomalously high concentration along sites SM and M5 with a gradual decreases in TSS concentration from the mouth of the Sabaki River seawards. Amongst the sites along the trend 1, site M1 showed minimal changes in TSS concentration over time. The high concentration for trend 3 is related to plume sediments from inland (continental denudation) showing a direct contribution of sediments sourced from the land. The results clearly indicate that TSS concentrations are variable at temporal scale of 15 minutes and the concentration levels are dependent partly on the location of the sites away from the land and partly on the location along the plume from the Sabaki River. These results attest to the novelty of the developed MSG code to monitor TSS concentration along the coastal environment at near-real time-resolution of 15minutes.

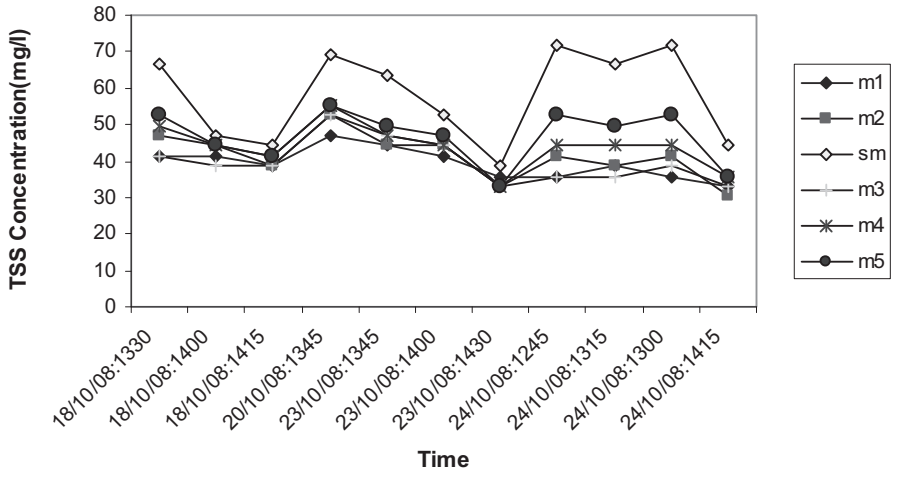

Figure 16 **Line graph showing the spatial-temporal variation of the TSS concentrations Modeled from the MSG TSS CODE for 11 images during the study period (18th-25th October 2008).**

5.1.5. Variations in TSS concentration with Respect To Turbidity, Bottom Depth, Chlorophyll-a, Salinity, Temperature, and Current Speed

An investigation was done to assess variations in the TSS concentration in respect to seven variable parameters taken from the validation site. Figure 17 and Table 9below shows line graphs indicating the TSS concentration variation over the study period in respect to turbidity (a), bottom depth (b), chlorophyll-a(c), salinity (d), temperature (e), and current speed (f). Although graph (a) clearly indicates clear positive relation (an increase in the TSS concentration led to an increase in turbidity) in the variation between the TSS concentration and Turbidity, the correlation coefficient was only 0.037 while the regression analysis was found to be 12%. An increase in bottom depth (graph (b)) led to an increase TSS concentration apart from in the reading made on 23rd October, 2008 which influenced the correlation coefficient to the negative (-0.60) but still high enough to indicate a strong relationship whose R^2 was observed to be 36%.

The current speed was observed to have a negative relationship such that an increase in the current speed led to a decrease in the TSS concentration. This is clearly depicted in the line graph (f). However, regression analysis shows that only 4.3% of the TSS concentration could be explained by the Current speed. A further investigation on to the correlation coefficient showed a negative ration of -0.21. Correlation coefficient show that an increase in chlorophyll-a concentration led to a decrease in the TSS concentration whose level was -0.032. However, the regression analysis was found to be 79% indicating that 79% of the TSS concentration could be explained by the chlorophyll concentration. A line graph of the same showed strong association where an increase in chlorophyll led to an increase in TSS concentration during the spring tide which shoots high 23rd October, 2008 and eventually becomes almost constant during the neap tide.

A high inverse relationship was observed be between the TSS concentration and salinity levels with a correlation coefficient of -0.75 and an R^2 of 57%. The line graph (d) as well showed clearly that an increase in salinity led to decrease in TSS concentration. A increase in temperature led to a decrease in the TSS concentration with a correlation coefficient of -0.108. This corresponded to an $R^{2\ of}$ 0.01%. The line graph (e) as well showed little variation of TSS concentration with respect to Temperature. TSS concentration varied positively in respect to Particulate Organic Matter (POM). This relationship was quantified with a correlation coefficient of 0.561 and a regression analysis of 31%. A line graph (f) indicated the same.

Table 9 **Table showing Regression analysis and correlation coefficient of modeled TSS with respect to turbidity (a), bottom depth (b), chlorophyll-a(c), salinity (d), temperature (e), and current speed (f).**

Related Parameter with TSS	**Correlation Coefficient**	**Regression Relationship**	**R2**
Secchi Disk Depth	0.037	y = 0.0027x3 - 0.3123x2 + 11.927x - 147.71	0.1204
Bottom Depth	-0.601	y = -0.193x + 15.482	0.3617
current speed	-0.205	y = -0.1024x + 7.9651	0.0425
chlorophyll	-0.032	y = 3E-05x3 - 0.0034x2 + 0.1293x - 1.6377	0.7907
salinity	-0.753	y = -0.2141x + 44.103	0.5717
Temperature	-0.108	y = -0.0359x + 29.331	0.0117
POM	0.561	y = 0.0005x - 0.0121	0.3145

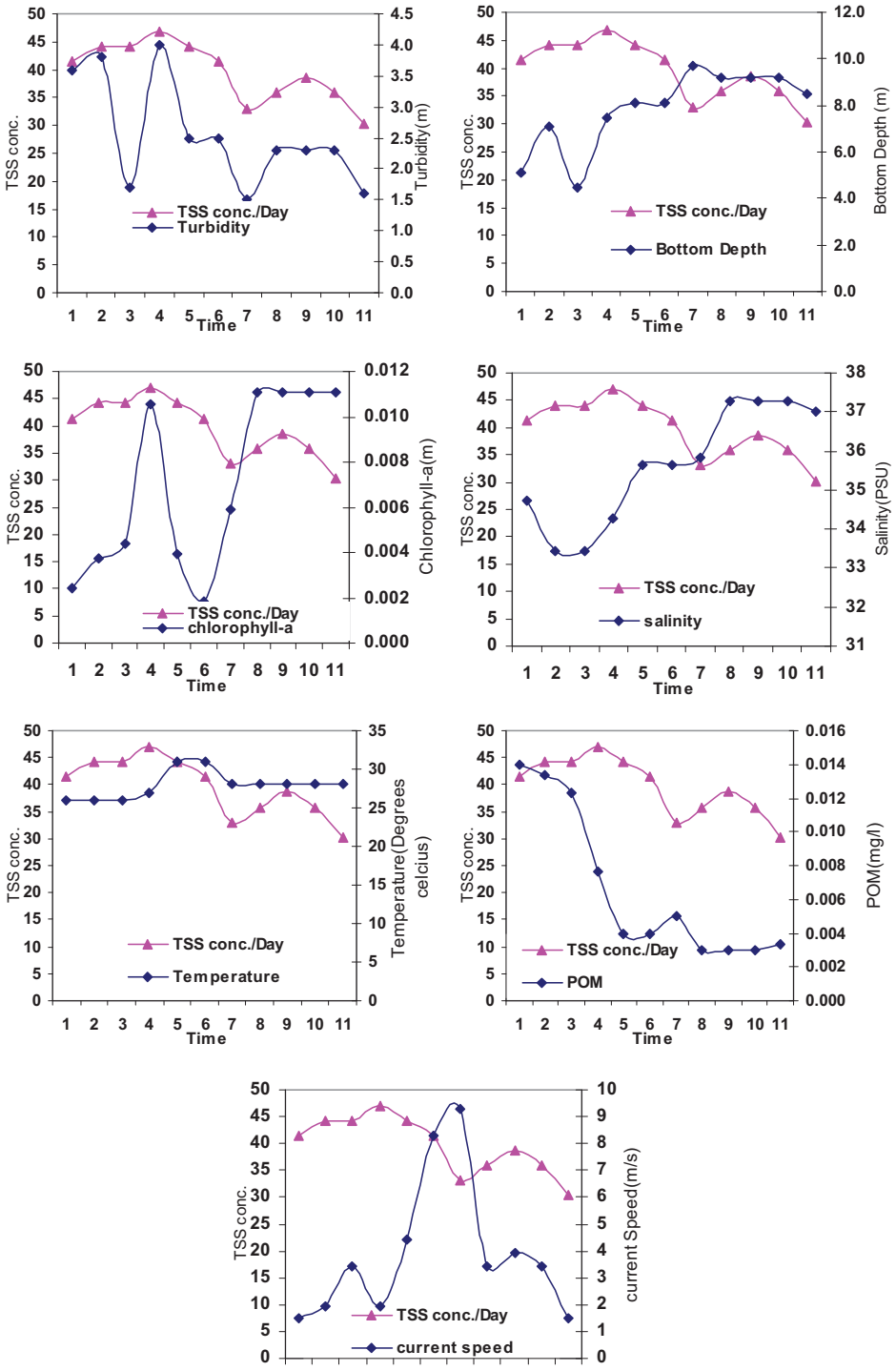

Figure 17 **Figure showing variations in TSS with respect to turbidity (a), bottom depth (b), chlorophyll-a(c), salinity (d), temperature (e), and current speed (f).**

5.1.6. Model Errors

Although the Total Suspended Sediments retrieved from MSG TSS CODE are very similar to field measurements of the plume, differences between the two data sources are likely. Root Mean Square Error (RMSE) was able to explain the differences between the measured and the modelled concentrations. The scatter plot of the modelled verses measured TSS concentration of small particles also depicted systematic as well as random error. However a statistical test showed that the Systematic error in the small particles was not significant. (Intercept test statistic, t=-1.181, SE= 5.234, P= 0.268) Since P-value was greater than 0.05. This means that the systematic error on the measured TSS concentration was not significant. A test on the slope showed a significance in systematic error (Slope test statistic, t= 7.120, SE=0.184, P= < 0.001) (Table 10) depicting that there was significant systematic errors on the modeled TSS concentration. This was as well observed in the large particles (Intercept test, t=-0.936, SE= 6.306, P= 0.374) while the slope test results in (slope test, t= 5.863, SE=0.159, P= < 0.001).

Table 10 **Table showing the significance test of the systematic error for small particles**

	B	Std. Error	Beta	t	Sig.
Coefficient	-6.181	5.234		-1.181	.268
Slope	1.312	.184	.922	7.120	.000

Table 11 **Table showing the significance test of the systematic error for large particles**

	B	Std. Error	Beta	t	Sig.
Coefficient	-5.905	6.306		-.936	.374
Slope	.932	.159	.890	5.863	.000

Both tests were done at 95% confidence intervals. The test statistic (t) quantification helped in deciding whether the null hypothesis (i.e. there is systematic error) would be rejected or not. This type of test was used due to the limitations in the number of validation points (Moore et al 2003). In this case it was calculated by dividing the estimated intercept or slope (denoted by (B) in this case) by the respective standard error. Significance which is denoted by *Sig.* (table 10 and 11) was used to test the probability that the test statistic will lead to rejecting of the null hypothesis when it's actually true. The P- value indicates how much evidence against null hypothesis. If P is smaller than the critical value (which is set at (0.05) in this case), it means that there is more evidence against the H_0 hypothesis. The null hypothesis is normally rejected if the P-value is less than the critical value.

6. Discussion

The main goal of this study was to adopt a bio-optical model for estimating the concentration of the Total Suspended Sediments. Though three models were tested for their ability to retrieve Total suspended sediments, only two are presented. This was because the Gordon *et al* (1975) resulted in negative values and is recommended when backscattering is assumed to be smaller than absorption (Muller *et al.,* 2003[c]).

6.1.1. Gordon et al., (1988) model and Morel and Prieur, (1977)

The Gordon *et al.,* (1988) model and Morel and Prieur, (1977) demonstrated good performance of bio-optical modelling on MSG remote sensed data with similar correlation coefficient and regression analysis results. The simulation of the algorithm for TSS concentration of large particles using Morel and Prieur, (1977), model had the highest RSME as compared to the rest and hence had the lowest rating in this study. This was followed by the TSS concentration for the small particles simulated using Gordon *et al* (1988) model with 8.64mg/m^3 lower. The results of the simulation of TSS concentration using Morel and Prieur, (1977) gave the lowest RMSE which had only 0.1mg/m^3 difference from the RMSE of the large particle of the Gordon *et al.,* (1988), model. The achievement of retrieval of TSS from MSG indicates robustness of the model towards near real time monitoring of TSS concentration from any part of MSG coverage area.

Despite the established relationships between the reflectance-TSS, which vary with change in particle properties such as grain size, composition and refraction index (Wozniak and Stramski 2004; Binding et al. 2005), results presented in this research indicated that it is possible to determine TSS concentration from both small and large particles without very significant differences.

In this study, correlation coefficient results and regression analysis of the modeled verses the insitu total suspended sediments concentrations were relatively high. This was in agreement with a recent study by Eleveld *et al*, (2008) which related remote sensed (SeaWifs) suspended particulate matter and Insitu measurements, using POWERS algorithm that resulted in an r^2 of 0.87 in 19 Dutch monitoring stations which is only 2% higher than the TSS retrieved from MSG. Komick *et al*., (2009) used bioptical modelling technique by modifying GSM01 model and achieved an r^2 of 0.933 for total suspended sediments which is 8% higher than TSS concentration retrieved from MSG TSS code. Pradhan, *et al.,* (2005) as well generated an algorithm for suspended sediments retrieval using IRS-P4

OCM (Ocean Colour Monitor) which showed an r^2 of 0.96 with insitu data in Bay of Bengal. This was 11% higher than the TSS retrieved from MSG which can be improved by incorporating more validation data. Other studies try to relate the water-leaving reflectance with suspended matter concentrations (Mishra, 2004; Yan*, et al*., 1998).

The good relationship between the retrieved and in-situ measurements including the temporal performance depicted by the results merits use of relatively simple model of (Gordon et al. 1975) and two bands, as a major contribution by providing quantitative TSS information along the coastal environments. In addition, this approach (TSS code) could be expanded to carry out batch processing of MGS images at 15 minutes temporal resolution in an automated way covering all the areas of MSG coverage. However, caution should be taken while extending the application of the TSS code by consideration local illumination effects.

6.1.2. Detection of the TSS from MSG

The success of the Models applied in this study may have possibly be attributed to extraction of TSS from MSG Image in cloud and sun glint free pixels, which were validated with the insitu measurements. The effect of white caps in the atmospheric correction was minimal because the spatial resolution (3km) of MSG which leads to averaging of the radiance over a wide area. It is also worth noting that the time difference between insitu data collection and the image acquisition was not more than twenty minutes in all the measurements. This may be related to the movement of the TSS within the same pixel during the sampling and image acquisition time. In addition, the bottom reflectance was almost negligible as explained by bottom depth of the sampling stations. Differences in illumination conditions may lead to inaccuracies in sediments retrieval, therefore the MSG TSS CODE was designed such that one the input parameters could be varied to suit the area of interest i.e. study area in this. This could be extended to other areas of the within the MSG coverage to ensure the processing is specific to those locations.

There were notable errors between the modeled and the measured TSS concentration. Some these errors could possibly be accounted by chlorophyll absorption whose relationship with TSS was found to be 3.4%. Errors in calibration parameters may have propagated among other image processing introducing errors like radiometric, calibration errors and illumination conditions (Saunders and Kriebel, 1988). In addition, other negligible errors include the effect of CDOM that affect modeled concentrations (Stumpf and Pennock, 1989).

Despite the fact that the sensors such MSG provide a surface optical signal used to determine TSS concentration, it is unlikely to provide a complete distribution of the TSS throughout the water column because no water leaving signal can be retrieved from below the optical depth (Deng and Li, 2003). The variations in TSS concentration within the entire vertical water column could be significant with highest concentrations found near the bed (McCandliss et al., 2002; Wild-Allen et al., 2002). Pleskachevsky et al., (2005) and Souza et al (2007) have developed relationships which take into consideration sub-surface variability in their models. This remains an area of research where more work should be endeavored.

6.1.3. Trends in TSS long the Kenya Coast

The retrieved TSS concentration along the Kenya Coast, similar to other coastal environments, can be related to continental erosion as well as hydrologic processes that vary with respect to various factors such as climatic erosion as well as morphological parameters (Wolfgang and Probst, 1996. The vast contribution of the TSS is fluviatile sources (river regimes) for example previous studies at Sabaki River Estuary (validation site) have estimated that freshwater discharge and sediment investigation was in the order of 2000 million m^3 and 2 million tonnes respectively (Obura, 2001). This influx of sediments forms a plume of high TSS concentrations as depicted by TSS levels at SM and M5 (Fig. 13). However, this concentration levels soon become regulated by tides, winds and ocean currents.

From the forgoing, it is apparent that the Total Suspended Sediments concentration varies as a function of tide, wind, spring-neap tidal cycles (Fig. 13). In is supported by the pevios studies that observed both peak fresh water discharge and sediments load in the months of May and November. This corresponded to high total suspended sediments ranging from 0.3-4.0 g/l with a peak of approximately 4.05 g/l in May 2002 (KMFRI, 2002). Organic sediment load ranged from 5.3 to 8,771 tons/day with the peak in May 2002. During these periods characterised by low winds the Sabaki River plume spreads up to about 2-3 km into the deep waters. from the shoreline and moves slowly at a mean speed of 0.4m/s, extending in a northward direction along the coastline (Brakel, 1984). It has been observed that during the southern monsoon, the Sabaki plume does not extend far to the south and rarely does it extend beyond Ras Vasco da Gama hence in essence does not destroy coral reef complex south of Malindi, which is less than 5 km from the mouth of Sabaki River. However, to the north Sabaki plume moves a relatively greater distance northward and hence no coral reef complexes have been established in the southern region of Ungwana Bay (KMFRI, 2002).

In terms of the sediment load the Sabaki River' contribution of the sediments to the Indian Ocean surpasses that of Tana River, which is the largest river in Kenya. This is because of the presence of power generation dams along Tana River traps most of the sediments (KMFRI, 2002).

7. Conclussion and Recommendation

This research has shown that Meteosat Second Generation (MSG) data provides reliable estimates of the TSS concentration along coastal environments. The use of the these remote sensing data sets provides not only a synoptic view of the near surface TSS concentrations but also a very high temporal resolution of the 15 minutes which could be used with a high degree of accuracy to infer the driving mechanism of the variation in TSS concentrations.

The results in Table 7 shows a close agreement of between the insitu and retrieved TSS concentrations indicating coastal water characterized by low concentrations along the shoreline and increasing concentration seawards. The only exception to the spatial distribution is in areas characterized by river plume that spreads sediments 2-3 km into to ocean. The estimation of the spatial-temporal sediment distribution along coastal environment will improve integrated resource management strategies especially in maintaining safe navigation routes, harbour access and dredging operations.

It is apparent that the validation points used in this study were not spread to cover a wide spatial extent required to test the stability of the model (TSS code) to retrieve TSS over such extensive areas. On this note, it is recommended that further validation points be selected particularly covering areas with regular in-situ TSS monitoring programme and over very extensive areas of MSG coverage. This is necessary to affirm the robustness of the selected algorithms.

In addition the use of the black pixel assumption in future application of the MSG TSS code which states that ocean component in the near- infrared spectral region has negligible water-leaving component (Siegel, *et al*. 2000) is recommendable. This can be accomplished using the channel 1.6 um of MSG. However, it should be noted that this method is not applicable in Case II waters because the water is affected by both Visible and Infrared spectra.

8. References

Ahn Y.H., Moon J.E., Gallegos S., (2001). Development of suspended particulate matter algorithms for ocean color remote sensing. Korean J. Remote Sensing, 17 (4), 285-295.

Albert A., and Gege P., (2006). "Inversion of irradiance and remote sensing reflectance in shallow water between 400 and 800 n for calculations of water and bottom properties." Applied Optics, Vol. 45 (N0. 10): 2331-2345.

Austin R.W., (1974). The remote sensing of spectral radiance from below the ocean surface. In: Optical Aspects of Oceanography, N.G. Jerlov and E.S. Nielson, Eds., pp 317-344.

Binding C.E., Bowers D.G., and Mitchelson-Jacob E.G., (2005). Estimating suspended sediment concentrations from ocean colour measurements in moderately turbid waters; the impact of variable particle scattering properties. Remote Sensing of Environment., 94(3): p. 373-383.

Brakel W.H, (1984). Seasonal dynamics of suspended sediment plumes from the Tana and Sabaki Rivers, Kenya: analysis of landsat imagery-Short communication. Remote-sensing of the Environment. Vol. 16, 165-175.

Brindley H. E, and Ignatov A., (2006). Retrieval of mineral aerosol optical depth and size information from Meteosat second generation SEVIRI solar reflectance bands. Remote Sensing of the Environent 102 344-363

Chernetskiy M., Shevyrnogov A., Shevnina S., Vysotskaya G. and Sidko A., (2009). Investigations of the Krasnoyarsk Reservoir waters based on the multispectral satellite data. Advances in Space Research, 43(2): 206-213.

Chomko R. M, H.R. Gordon, S. Maritorena, and Siegel D.A., (2002). Simultaneous determination of oceanic and atmospheric parameters for ocean color imagery by spectral optimization: A validation. Remote Sensing of Environment, 84(2): 208-220.

Clark D.K., Baker E.T., and Strong A.E., (1980). Upwelled Spectral Radiance Distribution in Relation to Particulate Matter in Sea Water, Boundary-Layer Meteor. 18, 287–298.

De Kok J.M., (1992). A three-dimensional finite difference model for computation of near-and far-field transport of suspended matter near a river mouth. Continental Shelf Research, 12 (5/6),625-642.

Dekker A.G., Peters S.W.M., Rijkeboer M. and Berghuis H., (1998). Analytical processing of multi-temporal SPOT and Landsat images. In: Proceedings of EARSeL Conference May 1998 in Enschede, Netherlands: Operational Remote Sensing for Sustainable Development, Balkema, Rotterdam, pp. 315–323

Deng, M., Li, Y., (2003). Use of seaWiFS imagery to detect three dimensional distribution of suspended sediment. International Journal of Remote Sensing 24 (3), 519-534.

Doerffer R., and Schiller H., (2002). A Neural Network based atmospheric correction procedure for theretrieval of water constituent's procedure for the retrieval of water constituents in turbid case II water from Meris data, in Proc. Ocean Optics XVI, Santa Fe.

Dunne T., (1979). Sedimnt yield and landuse in tropical catchments. Journal of hydrology, 42, 281-300.

Eleveld M.A., Pasterkamp R., van der Woerd H.J. and Pietrzak J.D., (2008). Remotely sensed seasonality in the spatial distribution of sea-surface suspended particulate matter in the southern North Sea. Estuarine, Coastal and Shelf Science, 80(1): 103-113.

ESA, (2004). Observing the Earth; Feature Meteosat Second Generation. 2004 -10-11 [cited 2008 2008-05-21]; Available from: http://www.esa.int/esaEO/GGGGEHCM8EC_index_0.html.

Fargion G.S. and Mueller J.L., (2000). Ocean Optics Protocols for Satellite Ocean Color Sensor Validation, Revision2, NASA TM 2001-209955, NASA Goddard Space Flight Center, Greenbelt, Maryland, 184.

Garver S. A., and Siegel D. A., (1997). Inherent optical property inversion of ocean color spectra and its biogeochemical interpretation: I. Time series from the Sargasso Sea, J. Geophys. Res., Volume 102: 18607-18625.

Giulietta S. F., and M uller J. L., (2000). Ocean Optics Protocols For Satellite Ocean Color Sensor Validation, Revision 2. National Aeronautical and Space administration. Greenbelt, Maryland 20771, Goddard Space Flight Space Center. NASA/TM-2000-209966.

Gordon H. R., (1997). Atmospheric correction of ocean color imagery in the earth observing system era J. Geophys. Res. 102 17081–106

Gordon H. R., and Boynton G. C., (1997). Radiance-irradiance inversion algorithm for estimating the absorption and backscattering coefficients of natural waters: homogeneous waters. Appl. Opt. 36, 2636–2641.

Gordon H. R., Brown O. B., Evans R. H., Brown J. W., Smith R. C., Baker K. S., and Clark D. K., (1988). A Semi-analytic Radiance Model of Ocean Color, J. Geophys. Res., 93(D9), 10,909–10,924.

Gordon H.R., Brown O.B., and Jacobs M.M., (1975). Computed Relationships Between the Inherent and Apparent Optical Properties of a Flat Homogeneous Ocean, Applied Optics 14, 417-427.

Gordon H.R., and Morel A., (1983). Remote Assessment of Ocean Color for Interpretation of Satellite Visible Imagery. A Review. Lecture Notes on Coastal and Estuarine Studies, Volume 4, Springer Verlag, New York, 114 pp.

Healy T., Wang Y., Healy J. A., (2002). Muddy coasts of the World: processes, Deposits and Functions. Proceeding in Marine Science, Vol. 4. Elsevier, Amsterdam, 556 pp.

Hoge F. E., and Lyon P. E., (2005). New tools for the study of oceanic eddies: Satellite derived inherent optical properties. Remote Sensing of Environment 95(4): 444-452

IOCCG, (2006). Remote Sensing of Inherent Optical Properties: Fundamentals, Tests of Algorithms, and Applications. Lee, Z.-P. (ed.). Reports of the International Ocean-Colour Coordinating Group. Dartmouth, Canada. No. 5.

Jeffrey S. W., Humphrey G. F., (1975). New spectrophotometric equation for determining chlorophyll a, b, c1 and c2, Biochem. Physiol. Pflanz., 167, 194-204

Jerlov N.G., (1976). Marine optics. Elsevier Scientific publishing Company, Amsterdam, The Netherlands 231pp.

Kenya Marine and Fisheries Research Institute (KMFRI), (2002). Current Status Of Trawl Fishery Of Malindi-Ungwana Bay, Report.

Kitheka J. U., Obiero M., and Nthenge P.,(2005) . River discharge, sediment transport and exchange in the Tana Estuary, Kenya. Estuarine, Coastal and Shelf Science, 63, 455-468.

Kitheka J. U., Ongwenyi G. S., and Mavuti K. M., (2003). Fluxes and exchange of suspended sediment in tidal inlets draining a degraded mangrove forest in Kenya. Estuarine, Coastal and Shelf Science, 56, 655-667.

Komick N. M., Costa M. P. F., and Gower J., (2009). Bio-optical algorithm evaluation for MODIS for western Canada coastal waters: An exploratory approach using in situ reflectance." Remote Sensing of Environment In Press, Corrected Proof.

Laane R.W.P.M., Sonneveldt H.L.A., Van der Weyden A.J., Loch J.P.G., Groeneveld G., (1999). Trends in the spatial and temporal distribution of metals (Cd, Cu, Zn and Pb) and organic compounds (PCBs and PAHs). Journal of Sea Research, 41(1-2), 1-17.

LaJollo F., Tannenbaum S. R., and Labuza T. P. (1971). "Reaction at Limited Water Concentration. 2. Chlorophyll Degradation." Journal of Food Science 36(6): 850-853.

Loisel H., and Stramski D., (2000). Estimation of the inherent optical properties of natural waters from the irradiance attenuation coefficient and reflectance in the presence of Raman scattering. Applied Optics Vol. 39, No. 18: 183001-3011

Lorenzen C. J., (1967). Determination of chlorophyll and phaeopigments: spectrophotometric equations, Limnology Oceanography, 12

Maritorena S., Siegel D. A., Peterson A. R., (2002). Optimization of a semi-analytical ocean color model for global-scale applications Appl. Optics, Volume 41: 2705-2714

McCandliss, R.R., Jones, S.E., Hearn, M., Latter, R., Jago, C.F., (2002). Dymanics of suspended particles in coastal waters (south North Sea) during spring bloom. Journal of Sea Research 47, 285-302.

McClanahan T. R., and Obura D., (1997). Sedimentation effects on shallow coral communities in Kenya. Journal of Experimental Marine Biology and Ecology, 209(1-2): 103-122.

McClanahan T. R., Steneck R. S., Pietri D., Cokos B., and Jones, S. (2005). Interaction between inorganic nutrients and organic matter in controlling coral reef communities in Glovers Reef Belize. Marine Pollution Bulletin, 50(5): 566-575.

Mishra A.K., (2004). Retrieval of suspended sediment concentration in the estuarine waters using IRS-1C WiFS data, International journal of applied earth observation and Geoinformation. 6, 83-95.

Mobley C. D., (1994). Light and water: radiative transfer in natural waters, San Diego : Academic Press, : 592 pg.

Moore D. S. and MCcabe G.P., (2003). Introduction to the practice of statistics, fourth Edition, Freeman, Newyork., 829p.

Morel A., (1974). Optical properties of pure water and pure sea water, chapter 1 in Optical Aspects of Oceanography, Edited by N.G. Jerlov and E.S. Nielsen, Academic Press, New York, 1-24.

Morel A., and Gentili B., (1996). Diffuse reflectance of oceanic waters: III implication of bidirectionality for the remote - sensing problem. Applied optics. 35(1996)24. pp. 4850-4862.

Morel A., and Prieur L., (1977). Analysis of variations in ocean color. Limnol. Oceanogr. 22. pp. 709-722.

Mueller J. L., Davis K. C., Kuwahara V. S., Lazin G., Brown S.W., Fargion G. S., Yarbrough M. A., Flora S., Broenkow W., Kim Y. S., Johnson B. C., Yuen M., (2003)[a]. Ocean Optics Protocols For Satellite Ocean Color Sensor Validation, Revision 4, Volume VI: Special Topics in Ocean Optics Protocols and Appendices. NASA/TM-2003-211621. G. S. F. a. C. R. M. James L. Mueller, Editors. Greenbelt, Maryland 20771, National Aeronautical and Space administration Goddard Space Flight Space Center. Rev4-Vol.VI.

Mueller J. L., Morel A., Frouin R., Davis C., Arnone R., Carder K., Lee Z.P., Steward R.G., Hooker S., Mobley D. C., Scott M., Holben B., Miller M., Pietras C., Knobelspiesse D. K., Fargion S. G., Porter J. and Voss K., (2003) [b]. Ocean Optics Protocols for Satellite Ocean Color Sensor Validation, Revision 4, Volume III: Radiometric Measurements and Data Analysis Protocols. G. S. F. a. C. R. M. James L. Mueller. Greenbelt, Maryland 20771, National Aeronautical and Space administration Goddard Space Flight Space Center. NASA/TM-2003-21621/Rev-Vol III

Mueller J.L. and Austin R.W., (1995). Ocean Optics Protocols for SeaWiFS Validation, Revision 1. NASA Tech. Memo. 104566, Vol. 25, S.B. Hooker and E.R. Firestone, Eds., NASA Goddard Space flight center, Greenbelt, Maryland, 66 pp.

Mueller J.L. and Fargion G.S., (2002). Ocean Optics Protocols for Satellite Ocean Color Sensor Validation, Revision 3, NASA TM 2002-210004, NASA Goddard Space Flight Center, Greenbelt, Maryland, 308pp.

Mueller J.L., and Austin R.W., (1992). Ocean Optics Protocols for SeaWiFS Validation. NASA Tech. Memo. 104566,Vol. 5, S.B. Hooker and E.R. Firestone, Eds., NASA Goddard Space flight center, Greenbelt, Maryland, 45 pp.

Mueller J.L., Davis, C.; Arnone R.., Frouin R., Carder K.., Lee Z.P., Steward R.G., Hooker S., Mobley, C.D., McLean S., (2003)[c]. Above-water radiance and remote sensing reflectance measurement and analysis protocols. In Ocean optics protocols for satellite ocean color sensor validation, rev. 4: Radiometric measurements and data analysis protocols; Mueller, J.L., Fargion, G.S., McClain, C.R., Eds.; NASA, NASA/TM-2003-21621/REV-VolIII.

Obura D. O., (2001). Kenya. Marine Pollution Bulletin 42(12): 1264-1278.

Ojany F. F., and Ogendo R.B, (1986). Kenya. A study in physical and human Geography. Longman, Kenya. Nairobi. 228.

Penndorf R., (1957). Tables of the Refractive Index for Standard Air and the Rayleigh Scattering Coefficient for the Spectral Region Between 0.2 and 20.0 Microns and their Application to Atmospheric Opt., J. Opt. Soc. Am., 47, 176-182.

Pierson D.C., and Strombeck,N., (2001). Estimation of radiance reflectance and the concentrations of optically active substances in Lake Malaren, Sweden, based.The Science of the Total Environment, 268 (1), p.171-188

Pleskachevsky, A., Gayer, G., Horstmann, J., Rosenthal, W., 2005. Synergy of satellite remote sensing and numerical modeling for monitoring of suspended particulate matter. Ocean Dynamics 55 (1), 2-9.

Pradhan Y., Thomaskutty A. V., Rajawat A. S., and Nayak S., (2005) Improved regional algorithm to retrieve total suspended particulate matter using IRS-P4 ocean colour monitor data. Pure Applied. Optics, 7: 343-349

Preisendorfer R.W., (1960). Recommendation on the standardization of concepts, terminology and notation of hydrologic optics. Scripps Inst. Of Oceanogr., SIO Report, 96pp.

Preisendorfer R.W., (1976). Hydrologic Optics, Vol 1. Washington, Dep. of Commerce.

Ruddick K. G., Ovidio F., Rijkeboer M., (2000). Atmospheric Correction of SeaWifs imagery for turbid coastal and inland waters. Applied Optics, 39: p. 897-912

Saunders R. W., and Kriebel K. T., (1988). An improved method for detecting clear sky and cloudy radiances from AVHRR data, Int. J. Remote Sens., 9, 123-150. (Correction, 1988, Int. J. remote Sens., 9, 1393-1394

SCOR/UNESCO, (1966), Determinations of photosynthetic pigments in seawater, Rep. SCOR/UNESCO WG 17, UNESCO Monogr. Oceanogr. Methodol., 1, Paris.

Short F.T. and Coles R.G. eds., (2001). Global Seagrass Research Methods. Elsevier Science B.V., Amsterdam. 473pp

Siegel D.A., Wang M., Maritorena S., and Robinson W. (2000). Atmospheric correction of satellite ocean color imagery: the black pixel assumption. Applied Optics, 39 : 3582 - 3591

Smith R.C., and Baker K., (1981). Optical properties of the clearest natural waters, Appl. Opt., 20(2), 177-184.

Souza A., Holt J., Proctor R., (2007). Modelling SPM on the NW European Shelf Seas. In Balson, P.S., Collins, M.B. (Eds), Coastal and shelf sediments Transport, Vol. 274. Geological Society of London, Special Publications, pp. 147-158.

Sterckx S., and Debruyn W., (2004). A hyperspectral view of the North Sea. in Proceedings of the Airborne Imaging Spectroscopy Workshop. Bruges

Strickland J. D. H., Parsons T. R., (1968). A practical handbook of seawater analysis. Pigment analysis, Bull. Fish. Res. Bd. Canada, 167

Stumpf R. P., and Pennock J. R., (1989). Calibration of a general optical equation for remote sensing of suspended sedimnts in moderately turbid estuary. Journal of Geophysical Research 94(10), 14,363-14,371.

Turner A., and Millward G.E., (2002). Suspended particles: their role in estuarine biogeochemical cycles. Estuarine, Coastal and Shelf Science 55, 857-883.

UNEP/GPA W., (2004). Overview of Physical Alteration and Destruction of Habitats in the Eastern African Region using Geographical Information System (GIS).

van Katwijk M. M., Meier N. F., van Loon R., van Hove E. M., Giesen W. B. J. T., G. van der Velde, and den Hartog C., (1993). Sabaki River sediment load and coral stress—Correlation between sediments and condition of the Malindi-Watamu reefs in Kenya (Indian-Ocean), Mar. Biol., 117, 675– 683.

Vermote E., Tanre D., Deuze J. L., Herman M., and Morcrette J. J., (1997). Second simulation of the satellite signal in the solar spectrum. An overview, IEEE Trans. Geosci. Remote Sensing, vol. 35, pp. 675-686.

Wang M., (2006). Effects of ocean surface reflectance variation with solar elevation on normalized water-leaving radiance. Applied Optics. 45(17):4122-8.

Wang D. , Feng X. , Ma R. and, Kang G., (2007). A method for retrieving water-leaving radiance from Landsat TM image in Taihu Lake, East China. Chinese Geographical Science Vol. 17, No.4, 364-369 pp.

Warrick J. A., Mertes L. A., Siegel D. A., (2004). Estimating suspended sediment concentrations in turbid coastal water of the Santa Barbara Channel ith SeaWiFS. Int. J. Remote Sensing, vol. 25 no. 1995-2002.

Wild-Allen K., Lane A., Tett P., (2002). Phytoplanktons, sediments and optical observations in Netherlands coastal water in spring. Journal of Sea Research 47, 303-315.

Winterwerp J.C., and Van Kesteren W.G.M., (2004). Introduction to the physics of Cohesive Sediments in the Marine Emvironment. Developments in Sedimentology 56. Elsevier, Amsterdam, 576pp.

Wolfgang L., and Probst J., (1996). Predicting the oceanic input of organic carbon by continental erosion. Global Biochemical Cycles, 10(1): p. 23-41.

Wozniak S.B., Stramski D., (2004). Modeling the optical properties of mineral particles suspended in seawater and their influence on ocean reflectance and chlorophyll estimation from remote sensing algorithms. Applied Optics. 43 (17), 3489-350

Yan L., Weia H., and Minga F., (1997). An algorithm for the retrieval of suspended sediment in coastal waters of China from AVHRR data. Continental Shelf Research 18(1998) 487-500.

Appendix 1: Table Showing the results of sampling

Date	TSS mg/l	Secchi Disk(m)	Bottom Depth(m)	chla-mg/m3	Salinity (PSU)	POM(g/l)	Temperature	Current Speed	Time
10/18/2008	34.67	3.6	5.1	0.4720	34.7200	0.0140	28	10.27	10:21
10/18/2008	37.00	3.8	7.1	0.5902	33.4467	0.0133	28	1.96	11:00
10/18/2008	34.00	1.7	4.5	0.5510	33.9800	0.0123	28	3.42	11:15
10/18/2008	34.67	4	12.1	0.5508	33.8833	0.0120	28	3.91	11:40
10/18/2008	36.33	7	19.6	0.9053	33.5667	0.0117	28	1.96	12:15
10/18/2008	33.33	4.5	15.6	0.6295	32.6467	0.0107	28	2.93	12:45
10/18/2008	29.67	7	18.6	0.7077	29.2433	0.0133	28	2.93	1:30
10/19/2008	30.33	3	5.3	0.6680	35.7267	0.0093	28	38.62	11:10
10/19/2008	36.00	2	7.4	0.6678	34.7667	0.0087	28	29.82	11:55
10/19/2008	29.33	2.8	4.7	0.4325	34.9067	0.0093	28	29.82	12:05
10/19/2008	31.67	3.5	12.1	0.8268	35.2767	0.0090	29	20.04	12:31
10/19/2008	35.67	4	8.8	0.6687	34.9300	0.0097	28		1:07
10/19/2008	34.00	4	15.4	0.6292	34.4500	0.0090	28		1:30
10/19/2008	34.00	4	19.7	1.0220	31.1800	0.0093	28		2:09
10/20/2008	31.00	3	7.5	1.0243	34.2767	0.0077	28	1.96	10:35
10/20/2008	34.67	2	8.5	0.8658	34.2633	0.0100	28	5.86	11:20
10/20/2008	36.00	1.8	5.6	0.6690	34.4667	0.0077	28	8.31	11:30
10/20/2008	26.33	3.5	13.3	0.5505	34.6533	0.0063	28	4.87	11:53
10/20/2008	26.67	5	20.4	1.2987	33.9900	0.0070	28	8.31	12:25
10/20/2008	30.67	3.7	19.5	0.5505	33.4633	0.0067	28	5.87	12:46
10/20/2008	25.67	6	19.1	0.8652	31.2800	0.0077	28	5.37	13:30
10/21/2008	32.33	2	8.5	1.1813	37.1267	0.0077	28	4.89	10:15
10/21/2008	31.00	3	8.7	0.7868	36.9667	0.0090	28	7.33	10:36
10/21/2008	30.67	2.5	7	1.4583	36.4267	0.0100	28	43.51	11:04
10/21/2008	31.00	2.5	15.4	0.7470	36.4867	0.0090	28	42.05	11:26

10/21/2008	33.33	3	10.2	0.4720	36.9767	0.0097	28	7.33	11:50
10/21/2008	32.33	5	16.2	0.6300	37.5300	0.0120	28	2.44	12:05
10/21/2008	34.67	5.5	20.2	1.0628	36.0933	0.0087	28	3.91	12:34
10/23/2008	27.33	1.5	8.1	0.6290	35.6333	0.0040	28	6.84	10:55
10/23/2008	27.33	4	9.7	0.3542	35.8500	0.0050	29	9.29	11:35
10/23/2008	27.00	2.6	7.7	0.5900	36.0900	0.0063	29	9.29	11:40
10/23/2008	27.00	2.9	15.4	0.4715	35.6267	0.0053	29	8.31	12:00
10/23/2008	27.00	3.2	11.2	0.7080	35.4833	0.0020	29	26.89	12:21
10/23/2008	26.67	3.7	17.2	0.6305	35.2133	0.0040	28	9.78	12:35
10/23/2008	25.67	7	20.6	0.6685	35.0200	0.0043	28		13:02
10/24/2008	25.67	2.3	9.2	0.5920	37.2900	0.0030	26	3.42	10:02
10/24/2008	28.00	1.6	8.5	0.3153	37.0033	-0.0033	27	1.47	10:37
10/24/2008	24.67	1.8	6.7	0.3542	37.3700	0.0053	27	1.96	10:45
10/24/2008	24.33	2.5	14.7	0.3927	37.2933	0.0020	27	1.96	11:05
10/24/2008	27.67	3.6	21.4	0.2755	37.2733	0.0033	27.5	1.47	11:25
10/24/2008	30.00	4	17.4	0.4325	36.8033	0.0030	27	1.96	11:45
10/24/2008	26.67	6	20.6	0.5897	36.3600	0.0040	26	0.98	12:10
10/25/2008	26.67	2	7.9	0.5505	36.1667	0.0040	29	4.40	10:15
10/25/2008	24.33	2.2	8.4	0.5895	36.4733	0.0047	28	0.97	10:50
10/25/2008	43.00	2.4	6.6	1.0237	36.7167	0.0053	29	1.47	10:57
10/25/2008	34.00	2.7	14.9	0.5505	36.2567	0.0220	26	3.91	11:25
10/25/2008	32.67	3	21.1	0.5102	36.2367	0.0027	27	1.97	11:40
10/25/2008	28.67	3.3	17.6	0.6688	36.2267	0.0053	27	2.44	12:10
10/25/2008	31.33	4.2	21.1	0.6682	36.1733	0.0013	28	5.38	12:40

Appendix 2 : Table Showing the results of sampling

Date	Station	vol filtered(l)	Acetone vol used(ml)		chla-mg/m3	Salinity	TSS (g/l)	POM(g/l)
10/18/2008	m1	1	10		0.2363	34.7	0.039	0.016
10/18/2008	m1	1	10		0.8249	34.59	0.034	0.014
10/18/2008	m1	1	10		0.3548	34.87	0.031	0.012
10/18/2008	m2	1	10		0.3548	33.17	0.032	0.011
10/18/2008	m2	1	10		0.7080	33.02	0.04	0.015
10/18/2008	m2	1	10		0.7080	34.15	0.035	0.014
10/18/2008	m3	1	10		0.3548	34.41	0.035	0.011
10/18/2008	m3	1	10		0.4710	33.92	0.033	0.014
10/18/2008	m3	1	10		0.8272	33.61	0.036	0.012
10/18/2008	m4	1	10		0.7088	34.01	0.035	0.012
10/18/2008	m4	1	10		0.4710	33.16	0.031	0.011
10/18/2008	m4	1	10		0.4725	34.48	0.043	0.013
10/18/2008	m5	1	10		0.8265	33.57	0.04	0.016
10/18/2008	m5	1	10		0.7080	33.52	0.031	0.008
10/18/2008	m5	1	10		1.1813	33.61	0.029	0.011
10/18/2008	m6	1	10		0.5903	32.67	0.029	0.01
10/18/2008	m6	1	10		0.8265	32.61	0.031	0.012
10/18/2008	m6	1	10		0.4717	32.66	0.029	0.01
10/18/2008	sm	1	10		0.4717	29.51	0.037	0.011
10/18/2008	sm	1	10		0.8257	29.21	0.037	0.014
10/18/2008	sm	1	10		0.8257	29.01	0.037	0.015
10/19/2008	m1	1	10		0.5887	35.56	0.03	0.012
10/19/2008	m1	1	10		0.2363	35.86	0.029	0.009
10/19/2008	m1	1	10		1.1790	35.76	0.032	0.007
10/19/2008	m2	1	10		0.9428	33.98	0.033	0.012
10/19/2008	m2	1	10		0.5887	35.41	0.025	0.006
10/19/2008	m2	1	10		0.4718	34.91	0.03	0.008
10/19/2008	m3	1	10		0.4718	34.95	0.026	0.006
10/19/2008	m3	1	10		0.4718	35.2	0.034	0.01
10/19/2008	m3	1	10		0.3540	34.57	0.035	0.012
10/19/2008	m4	1	10		0.7080	34.92	0.031	0.01
10/19/2008	m4	1	10		1.1812	35.71	0.033	0.008
10/19/2008	m4	1	10		0.5910	35.2	0.043	0.009
10/19/2008	m5	1	10		1.1804	34.92	0.032	0.008
10/19/2008	m5	1	10		0.4717	34.81	0.035	0.009
10/19/2008	m5	1	10		0.3540	35.06	0.035	0.012
10/19/2008	m6	1	10		0.7072	34.41	0.034	0.008
10/19/2008	m6	1	10		0.5895	34.68	0.035	0.012
10/19/2008	m6	1	10		0.5910	34.26	0.033	0.007
10/19/2008	sm	1	10		0.8257	31.31	0.034	0.008
10/19/2008	sm	1	10		1.0613	31.57	0.037	0.011
10/19/2008	sm	1	10		1.1790	30.66	0.037	0.009
10/20/2008	m1	1	10		0.9442	34.37	0.03	0.008
10/20/2008	m1	1	10		1.0650	34.3	0.031	0.006
10/20/2008	m1	1	10		1.0635	34.16	0.032	0.009

10/20/2008m2	1	10	0.9450	34.05	0.037	0.012
10/20/2008m2	1	10	0.9435	34.37	0.039	0.011
10/20/2008m2	1	10	0.7088	34.37	0.032	0.007
10/20/2008m3	1	10	0.5895	34.48	0.027	0.008
10/20/2008m3	1	10	0.8273	34.19	0.029	0.009
10/20/2008m3	1	10	0.5902	34.73	0.023	0.006
10/20/2008m4	1	10	0.3540	34.76	0.026	0.007
10/20/2008m4	1	10	0.5895	34.57	0.028	0.006
10/20/2008m4	1	10	0.7080	34.63	0.026	0.006
10/20/2008m5	1	10	1.1804	34.39	0.033	0.008
10/20/2008m5	1	10	0.8241	33.91	0.028	0.006
10/20/2008m5	1	10	1.8915	33.67	0.031	0.007
10/20/2008m6	1	10	0.5895	32.79	0.026	0.007
10/20/2008m6	1	10	0.2355	34.06	0.026	0.007
10/20/2008m6	1	10	0.8265	33.54	0.025	0.006
10/20/2008sm	1	10	1.0635	31.39	0.041	0.009
10/20/2008sm	1	10	0.7080	30.9	0.029	0.006
10/20/2008sm	1	10	0.8242	31.55	0.034	0.008
10/21/2008m1	1	10	0.5910	36.77	0.029	0.005
10/21/2008m1	1	10	1.1804	37.76	0.03	0.009
10/21/2008m1	1	10	1.7723	36.85	0.038	0.009
10/21/2008m2	1	10	0.5895	37.25	0.03	0.009
10/21/2008m2	1	10	0.5910	36.13	0.028	0.01
10/21/2008m2	1	10	1.1798	37.52	0.034	0.008
10/21/2008m3	1	10	2.0100	37.06	0.028	0.009
10/21/2008m3	1	10	1.4213	35.96	0.032	0.011
10/21/2008m3	1	10	0.9435	36.26	0.033	0.01
10/21/2008m4	1	10	0.7064	36.5	0.03	0.009
10/21/2008m4	1	10	0.8257	36.4	0.034	0.008
10/21/2008m4	1	10	0.7088	36.56	0.036	0.01
10/21/2008m5	1	10	0.3540	36.96	0.035	0.01
10/21/2008m5	1	10	0.4725	37.06	0.029	0.008
10/21/2008m5	1	10	0.5895	36.91	0.033	0.011
10/21/2008m6	1	10	0.4725	37.28	0.036	0.014
10/21/2008m6	1	10	0.5895	37.72	0.035	0.011
10/21/2008m6	1	10	0.8280	37.59	0.033	0.011
10/21/2008sm	1	10	1.0628	36.06	0.029	0.008
10/21/2008sm	1	10	0.9450	35.96	0.035	0.01
10/21/2008sm	1	10	1.1806	36.26	0.029	0.008
10/23/2008m1	1	10	0.8265	35.41	0.026	0.004
10/23/2008m1	1	10	0.4710	35.76	0.029	0.004
10/23/2008m1	1	10	0.5895	35.73	0.027	0.004
10/23/2008m2	1	10	0.4717	35.87	0.027	0.005
10/23/2008m2	1	10	0.1185	36.14	0.028	0.006
10/23/2008m2	1	10	0.4725	35.54	0.026	0.004
10/23/2008m3	1	10	0.5910	36.11	0.028	0.005
10/23/2008m3	1	10	0.7072	36.06	0.025	0.005
10/23/2008m3	1	10	0.4717	36.1	0.028	0.009
10/23/2008m4	1	10	0.4725	35.88	0.025	0.003
10/23/2008m4	1	10	0.3509	35.95	0.029	0.008
10/23/2008m4	1	10	0.5911	35.05	0.027	0.005
10/23/2008m5	1	10	0.7080	35.65	0.026	0.002
10/23/2008m5	1	10	0.4718	35.26	0.024	0.002
10/23/2008m5	1	10	0.9442	35.54	0.03	0.002

10/23/2008m6	1	10	0.4725	35.44	0.028	0.004
10/23/2008m6	1	10	0.9458	35.05	0.025	0.004
10/23/2008m6	1	10	0.4733	35.15	0.024	0.004
10/23/2008sm	1	10	0.7080	35.01	0.027	0.002
10/23/2008sm	1	10	0.8258	34.96	0.029	0.006
10/23/2008sm	1	10	0.4717	35.09	0.026	0.005
10/24/2008m1	1	10	0.1244	37.09	0.024	0.003
10/24/2008m1	1	10	0.9442	37.16	0.025	0.002
10/24/2008m1	1	10	0.7073	37.62	0.028	0.004
10/24/2008m2	1	10	0.2363	37.03	0.02	-0.013
10/24/2008m2	1	10	0.3548	36.87	0.024	0.001
10/24/2008m2	1	10	0.3548	37.11	0.03	0.002
10/24/2008m3	1	10	0.3532	37.18	0.026	0.005
10/24/2008m3	1	10	0.3548	37.46	0.02	0.005
10/24/2008m3	1	10	0.3548	37.47	0.027	0.006
10/24/2008m4	1	10	0.4710	37.43	0.024	0.003
10/24/2008m4	1	10	0.2355	37.35	0.035	0.001
10/24/2008m4	1	10	0.4718	37.1	0.024	0.002
10/24/2008m5	1	10	0.3548	37.34	0.028	0.003
10/24/2008m5	1	10	0.2363	37.24	0.029	0.005
10/24/2008m5	1	10	0.2355	37.24	0.033	0.002
10/24/2008m6	1	10	0.2363	36.88	0.025	0.001
10/24/2008m6	1	10	0.3548	36.74	0.026	0.004
10/24/2008m6	1	10	0.7064	36.79	0.029	0.004
10/24/2008sm	1	10	0.5903	36.88	0.024	0.003
10/24/2008sm	1	10	0.4717	36.05	0.028	0.004
10/24/2008sm	1	10	0.7072	36.15	0.032	0.005
10/25/2008m1	1	10	0.5895	35.73	0.026	0.004
10/25/2008m1	1	10	0.5902	36.43	0.028	0.004
10/25/2008m1	1	10	0.4717	36.34	0.026	0.004
10/25/2008m2	1	10	0.5887	36.59	0.076	0.004
10/25/2008m2	1	10	0.7087	36.83	0.028	0.005
10/25/2008m2	1	10	0.4710	36	0.025	0.005
10/25/2008m3	1	10	0.7087	36.69	0.028	0.003
10/25/2008m3	1	10	0.5879	36.72	0.038	0.007
10/25/2008m3	1	10	1.7745	36.74	0.036	0.006
10/25/2008m4	1	10	0.7095	36.4	0.034	0.004
10/25/2008m4	1	10	0.4710	35.97	0.03	0.004
10/25/2008m4	1	10	0.4710	36.4	0.094	0.058
10/25/2008m5	1	10	0.4710	36.49	0.029	0.002
10/25/2008m5	1	10	0.4702	36	0.029	0.003
10/25/2008m5	1	10	0.5895	36.22	0.028	0.003
10/25/2008m6	1	10	1.0621	36.02	0.029	0.004
10/25/2008m6	1	10	0.4717	36.24	0.028	0.006
10/25/2008m6	1	10	0.4725	36.42	0.037	0.006
10/25/2008sm	1	10	0.4710	35.71	0.026	0.001
10/25/2008sm	1	10	0.8257	36.46	0.024	0.002
10/25/2008sm	1	10	0.7080	36.35	0.023	0.001

Appendix 3 : Table Showing the Significance Test of the Differences

One-Sample Test

	Test Value = 0					
	t	df	Sig. (2-tailed)	Mean Difference	95% Confidence Interval of the Difference	
					Lower	Upper
Tss Conc.(Mg/l)(springtide)	42.470	20	.000	32.5396825	30.941469	34.137896
Tss Conc.(Mg/l)(neaptide)	30.129	20	.000	28.4603175	26.489865	30.430770

One-Sample Test

	Test Value = 0					
	t	df	Sig. (2-tailed)	Mean Difference	95% Confidence Interval of the Difference	
					Lower	Upper
bottom-depth(springtide)	9.252	20	.000	11.9000	9.217	14.583
Bottom-Depth(neaptide)	11.315	20	.000	13.6190	11.108	16.130

One-Sample Test

	Test Value = 0					
	t	df	Sig. (2-tailed)	Mean Difference	95% Confidence Interval of the Difference	
					Lower	Upper
Secchi Disk(neaptide)	10.600	20	.000	3.1667	2.543	3.790
secchi disks(springtide)	11.648	20	.000	3.8048	3.123	4.486

Appendix 4 High-Low Prediction For Mombasa Station Latitude 4˚4's Longitude 39˚39'e October 2008

HL	DATE				Time	HGT.	Time	HGT.	Time	HGT.
0	Wed	1	10	08	505	3.7	1113	0.2	2314	0.4
0	Thu	2	10	08	532	3.6	1142	0.3	2340	0.5
0	Fri	3	10	08	558	3.5	1212	0.5	6	0.7
0	Sat	4	10	08	625	3.3	1243	0.7	33	0.9
0	Sun	5	10	08	653	3.1	1316	0.9	102	1.1
0	Mon	6	10	08	726	2.8	1358	1.2	139	1.4
0	Tue	7	10	08	813	2.6	1503	1.4	247	1.6
1	Wed	8	10	08	948	2.4	1713	1.5	-	-
1	Thu	9	10	08	531	1.7	1209	2.4	120	2.4
1	Fri	10	10	08	711	1.4	1323	2.6	203	2.7
1	Sat	11	10	08	801	1.1	1410	2.9	236	3
0	Sun	12	10	08	839	0.8	1448	3.1	-	-
0	Mon	13	10	08	307	3.3	913	0.5	2119	0.5
0	Tue	14	10	08	338	3.6	946	0.3	2149	0.4
0	Wed	15	10	08	409	3.8	1020	0.1	2220	0.3
0	Thu	16	10	08	442	3.9	1055	0.1	2253	0.3
0	Fri	17	10	08	516	3.9	1132	0.1	2328	0.4
0	Sat	18	10	08	553	3.8	1212	0.3	6	0.6
0	Sun	19	10	08	633	3.6	1256	0.6	49	0.8
0	Mon	20	10	08	720	3.2	1349	0.9	143	1.1
0	Tue	21	10	08	822	2.9	1501	1.1	-	-
1	Wed	22	10	08	309	1.4	1001	2.6	2319	2.4
1	Thu	23	10	08	519	1.4	1151	2.6	48	2.6
1	Fri	24	10	08	657	1.2	1309	2.8	145	3
1	Sat	25	10	08	757	0.9	1405	3	228	3.2
1	Sun	26	10	08	840	0.7	1449	3.1	-	-
0	Mon	27	10	08	305	3.5	917	0.5	2119	0.5
0	Tue	28	10	08	338	3.6	951	0.3	2150	0.5
0	Wed	29	10	08	409	3.7	1022	0.3	2219	0.5
0	Thu	30	10	08	438	3.6	1053	0.3	2248	0.5
0	Fri	31	10	08	506	3.6	1123	0.4	2316	0.6

(0-sping 1-Neap)

Appendix 5: MSG TSS CODE

```
%%%%%%%%%%%%%%%%%%%%%%%%%%%%%%%%%%%%%%%%%%%%%%%%%%%%%%%%%%%%%%%%%%%%%%%%%%%%
% MSG SPM CODE            =   calculate_SPM_concentrations(band1, band2)
% version 1.0
% last changes made on
% 2008-17-01                by Jane Ndungu (Msc Student),
%                           Dr. ir. Suhyb Salama(Supervisor),
%                                  Dr. Ben Mathias (Supervisor) and
%                           Joris Timmermans (Matlab Advisor)
% written code for retrieving suspended sediments concentrations
%
% This function only works with MSG bands (1,2).
%%%%%%%%%%%%%%%%%%%%%%%%%%%%%%%%%%%%%%%%%%%%%%%%%%%%%%%%%%%%%%%%%%%%%%%%%%%%

function [cx,bb_,R_0_min_,L_WN_ex_,L_WN_]              =   calculate_spm_concentrations(band1, band2)


if nargin~=2
    fprintf(1,'Error\nYou have to specify two bands as inputs (do not use this function as standalone script)\n')
    return
end

%% Sun parameters
cos_tts                          =   0.984807753;                          % cos of sun zenith angle

J                                =   292;                                  % Julian day
do_d                             =   1 + 0.0167*cos((2*pi*(J-3)) / 365);   % ratio of mean and actual earth-sun distance

%% Parameters
wl                               =   [635, 810];                           % wavelength

a_                               =   [0.119, 0.080];                       % atmospheric contribution to measured radiance (635,810)
tau_R_                           =   [0.05866, 0.02130];                   % Rayleigh optical thickness (635,810)
tau_03_                          =   [0.00000, 0.00000];                   % Ozone optical thickness, (We assume it has no effect)
R_0_                             =   [0.529, 0.529];                       % Reflection
R_                               =   [0.460, 0.460];                       % Refraction
f_0_                             =   [0.33,  0.33];                        % scattering contribution of sun angle=0
Q_0_                             =   [3.5,   3.5];                         % scattering contribution of sun angle=0
f_Q_                             =   [0.092, 0.092];                       % ratio of scattering contribution
Q_n_                             =   [3.75,  3.75];                        % Ratio of irradiance to any (direct / diffuse) radiance
F_0_mean_                        =   [1.8, 1.2];                           % Extra terrestrial solar irradiance

bsw_(1)                          =   0.00105;                              % backscattering of seawater
```

```
bsw_(2)                         =   0.00040;                            % backscattering of seawater
bbx_                            =   8.6;                                % specific backscattering coefficient of suspended matter
f_Q_0_(1)                       =   f_0_(1) / Q_0_(1);                  % ratio of scattering contribution at sun angle=0
f_Q_0_(2)                       =   f_0_(2) / Q_0_(2);                  % ratio of scattering contribution at sun angle=0
l_                              =    0.0949;

% Absorption related parameters
a_h20_                          =   [0.324, 2.070];                     %  light absorption of water
a_chl_                          =   [0.001500, 0.000];                  %  light absorption of chlorophyll

a_tot_                          =   a_h20_ + a_chl_;                    % total light absorption

%% Computations
% Atmospheric correction
atmc_(1)                    =  ((a_(1)*F_0_mean_(1))/pi);                  % converting atmospheric path reflectance to Radiance
atmc_(2)                    =  ((a_(2)*F_0_mean_(2))/pi);                  % converting atmospheric path reflectance to Radiance

L_w1_(:,:,1)                =   band1-atmc_(1);                                    % water leaving radiance (atmosphere corrected)
L_w1_(:,:,2)                =   band2-atmc_(2);                                    % water leaving radiance (atmosphere corrected)


tau_atm_(1)                 =   exp((1/2*(tau_R_(1) + tau_03_(1))) / cos_tts );    % atmospheric transmission
tau_atm_(2)                 =   exp((1/2*(tau_R_(2) + tau_03_(2))) / cos_tts );    % atmospheric transmission

% calculation of normalized water leaving radiance
L_WN_(:,:,1)                =   L_w1_(:,:,1) / (tau_atm_(1)*do_d);
L_WN_(:,:,2)                =   L_w1_(:,:,2) / (tau_atm_(2)*do_d);

% calculation of Exact water leaving radiances
L_WN_ex_(:,:,1)             =   L_WN_(:,:,1) * (R_0_(1)/R_(1))* f_Q_0_(1) * 1/f_Q_(1); % bidirectional reflection corrected
L_WN_ex_(:,:,2)             =   L_WN_(:,:,2) * (R_0_(2)/R_(2))* f_Q_0_(2) * 1/f_Q_(2); % bidirectional reflection corrected

% calculation of subsurface irradiance reflectance
R_0_min_(:,:,1)             =   L_WN_ex_(:,:,1) * Q_n_(1) / (F_0_mean_(1)*R_0_(1));
R_0_min_(:,:,2)             =   L_WN_ex_(:,:,2) * Q_n_(2) / (F_0_mean_(2)*R_0_(2));

% calculation of suspended sediments backscattering
bb_(:,:,2)                  =  a_tot_(2)*R_0_min_(:,:,2)./(Q_n_(2)*l_) ;     % total backscattering coefficient
bb_(:,:,1)                  =   bb_(:,:,2)*(((wl(2))/(wl(1)))^1.7);
cx                          =  ((bb_(:,:,1)-(0.5*bsw_(1)))/(bbx_));          % concentration of total suspended sediments

% keyboard
return
```